

AD-A128 577

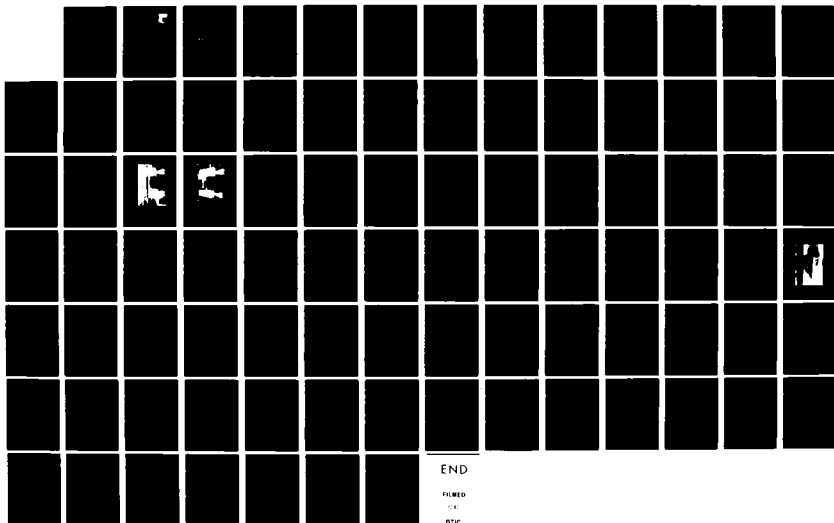
AN AUTOMATED DUAL HORN-REFLECTOR MICROWAVE ABSORBER  
MEASUREMENT SYSTEM VOL. (U) AIR FORCE WRIGHT  
AERONAUTICAL LABS WRIGHT-PATTERSON AFB OH 8 KENT  
JUN 82 AFWAL-TR-81-1284-VOL-1

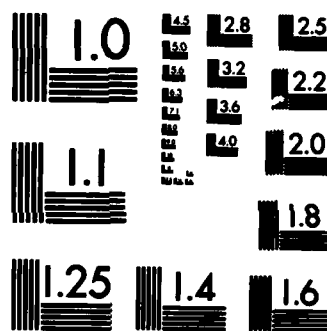
1/1

UNCLASSIFIED

F/G 14/2

NL





MICROCOPY RESOLUTION TEST CHART  
NATIONAL BUREAU OF STANDARDS-1963-A

AFWAL-TR-81-1284  
Volume I



# AN AUTOMATED DUAL HORN-REFLECTOR MICROWAVE ABSORBER MEASUREMENT SYSTEM

Brian Kent

June 1982

Interim Report for Period 15 June 1981 - 15 September 1981

Approved for public release; distribution unlimited.

AVIONICS LABORATORY  
AIR FORCE WRIGHT AERONAUTICAL LABORATORIES  
AIR FORCE SYSTEMS COMMAND  
WRIGHT-PATTERSON AIR FORCE BASE, OHIO 45433

A

098

AD A120577

DTIC FILE COPY

NOTICE

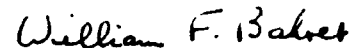
When Government drawings, specifications, or other data are used for any purpose other than in connection with a definitely related Government procurement operation, the United States Government thereby incurs no responsibility nor any obligation whatsoever; and the fact that the government may have formulated, furnished, or in any way supplied the said drawings, specifications, or other data, is not to be regarded by implication or otherwise as in any manner licensing the holder or any other person or corporation, or conveying any rights or permission to manufacture use, or sell any patented invention that may in any way be related thereto.

This report has been reviewed by the Office of Public Affairs (ASD/PA) and is releasable to the National Technical Information Service (NTIS). At NTIS, it will be available to the general public, including foreign nations.

This technical report has been reviewed and is approved for publication.

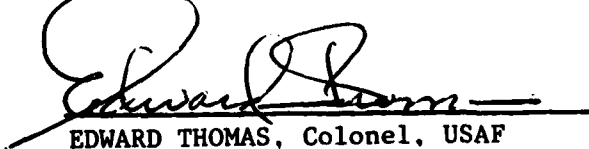


BRIAN M. KENT, Elec Engr  
Passive ECM Br, EW Division  
Avionics Laboratory



WILLIAM F. BAHRET, Chief  
Passive ECM Br, EW Div  
Avionics Laboratory

FOR THE COMMANDER:



EDWARD THOMAS, Colonel, USAF  
Chief, Electronic Warfare Division  
Avionics Laboratory

"If your address has changed, if you wish to be removed from our mailing list, or if the addressee is no longer employed by your organization please notify AFWAI/AAWP-3 W-PAFB, OH 45433 to help us maintain a current mailing list".

Copies of this report should not be returned unless return is required by security considerations, contractual obligations, or notice on a specific document.

Unclassified

SECURITY CLASSIFICATION OF THIS PAGE (When Data Entered)

REPORT DOCUMENTATION PAGE		READ INSTRUCTIONS BEFORE COMPLETING FORM
1. REPORT NUMBER AFWAL-TR-81-1284, Volume I	2. GOVT ACCESSION NO. AD-A120 577	3. RECIPIENT'S CATALOG NUMBER
4. TITLE (and Subtitle) AN AUTOMATED DUAL HORN-REFLECTOR MICROWAVE ABSORBER MEASUREMENT SYSTEM ✓		5. TYPE OF REPORT & PERIOD COVERED Interim 15 Jun-15 Sep 81
		6. PERFORMING ORG. REPORT NUMBER
7. AUTHOR(s) Brian Kent		8. CONTRACT OR GRANT NUMBER(s)
9. PERFORMING ORGANIZATION NAME AND ADDRESS Avionics Laboratory (AFWAL/AAWP) Air Force Wright Aeronautical Laboratories (AFSC) W-PAFB, OH 45433		10. PROGRAM ELEMENT, PROJECT, TASK AREA & WORK UNIT NUMBERS 76331309
11. CONTROLLING OFFICE NAME AND ADDRESS Avionics Laboratory (AFWAL/AAW) Air Force Wright Aeronautical Laboratories (AFSC) W-PAFB, OH 45433		12. REPORT DATE June 1982
		13. NUMBER OF PAGES 91
14. MONITORING AGENCY NAME & ADDRESS (if different from Controlling Office)		15. SECURITY CLASS. (of this report) Unclassified
		15a. DECLASSIFICATION/DOWNGRADING SCHEDULE
16. DISTRIBUTION STATEMENT (of this Report) Approved for public release; distribution unlimited.		
17. DISTRIBUTION STATEMENT (of the abstract entered in Block 20, if different from Report)		
18. SUPPLEMENTARY NOTES *AFWAL-TR-81-1284, Volume II contains computer software; therefore distribution is limited in accordance with AFR 300-6 (DOD Dir 4160.19 dtd 5 Apr 73). No DOD requests must include the statement of terms and conditions contained in Atch 21 to AFR 300-6.		
19. KEY WORDS (Continue on reverse side if necessary and identify by block number) permittivity permeability horn-reflector scattering parameter		
20. ABSTRACT (Continue on reverse side if necessary and identify by block number) In recent years, extreme interest has been shown in materials which absorb electromagnetic energy in the microwave and millimeter frequency bands. One of the primary methods of evaluating Radar Absorbing Materials (RAM) is to obtain the electrical and magnetic constants of permittivity ( $\epsilon$ ) and permeability ( $\mu$ ) of the material from which the RAM is constructed. Usually, the ( $\mu, \epsilon$ ) of a typical microwave absorber varies strongly as a function of frequency. Hence, in order to evaluate the performance of a wide band microwave absorber, it would be desirable to design and build a system which measures ( $\mu, \epsilon$ ) across a wide		

DD FORM 1 JAN 73 1473

EDITION OF 1 NOV 68 IS OBSOLETE

Unclassified

SECURITY CLASSIFICATION OF THIS PAGE (When Data Entered)

Unclassified

SECURITY CLASSIFICATION OF THIS PAGE(When Data Entered)

20. Abstract (Contd)

frequency band. *ex 16*

*mean*  
The Dual Horn-Reflector Microwave Absorber Measurement System discussed herein obtains the  $(\mu, \epsilon)$  of a homogeneous rectangular sample of material from 12.6 - 18.0 Gigahertz by measuring the scattering parameters  $S_{11}(\omega)$  and  $S_{21}(\omega)$  from the sample directly in the Frequency Domain. The overall accuracy of this measurement system is five to ten percent. *←*

Unclassified

SECURITY CLASSIFICATION OF THIS PAGE(When Data Entered)



TABLE OF CONTENTS

SECTION	PAGE
Volume I	
I INTRODUCTION	1
II THEORY BEHIND FREQUENCY DOMAIN MEASUREMENTS OF PERMITTIVITY AND PERMEABILITY	4
III THEORETICAL AND PRACTICAL SCATTERING PARAMETER MEASUREMENT TECHNIQUES USING ACCURACY ENHANCEMENT MODELLING	25
IV AUTOMATED FREQUENCY DOMAIN MATERIAL MEASUREMENT SYSTEM	44
V SUMMARY AND CONCLUSIONS	72
APPENDIX A ENGINEERING DRAWINGS OF DUAL HORN-REFLECTOR/SAMPLE HOLDER	73
REFERENCES	80
Volume II	
APPENDIX B COMPLETE LISTINGS OF PROGRAM CALNA AND PROGRAM FDMSP	82
APPENDIX C STANDARD OPERATING PROCEDURE FOR PROGRAMS CALNA AND FDMSP	132



# LIST OF ILLUSTRATIONS

FIGURE		PAGE
1	Geometry of Infinite Slab Problem	5
2	Potential Sample Holder Arrangements	12
3	Dual Horn-Reflector Sample Holder Test Set-Up	15
4	Geometry of Parabolic Reflector and Horn-Reflector Antennas	17
5	Variation of Horn-Reflector Shape with Focus Change	19
6	Photograph of Antenna/Sample Holder with Top Cover in Place	21
7	Photograph of Antenna/Sample Holder with Cover Removed and Teflon Sample in Place	22
8	Idealized Scattering Parameter Reflectometer	26
9	Frequency Dependence of a Typical 20dB Directional Coupler	28
10	Modelling the Non-Ideal One-Port Reflectometer	30
11	Modelling the Non-Ideal Two-Port Reflectometer	34
12	Flow Diagram for the Two-Port Error Model	35
13	Measuring the Leakage Error Term $e_{30}$	39
14	Measurement Set-up for the Transmission Error Parameters $e_{22}$ and $e_{10}e_{32}$	40
15	Finalized Frequency Domain Material Measurement System	45
16	Photograph of Dual Horn-Reflector/Sample Holder Reflectometer	46
17	Flowchart of Program CALNA	49
18	Flowchart of Program FDMSP	50
19	VSWR Test Set-Up	52
20	VSWR of Dual Horn-Reflector Before and After the Insertion of FGM-40 Tabs	53

LIST OF ILLUSTRATIONS (Concluded)

FIGURE		PAGE
21	Location of Absorber Tabs Used to Reduce VSWR	55
22	Test and Evaluation Set-Up for Reflect Error Parameter Model	57
23	Mu-Epsilon of Air (Frequency Domain)	60
24	Mu-Epsilon of Teflon (Frequency Domain)	61
25	Mu-Epsilon of Teflon (Time Domain)	62
26	Mu-Epsilon of Plexiglas (Frequency Domain)	64
27	Mu-Epsilon of Plexiglas (Time Domain)	65
28	Mu-Epsilon of Fiberglass (Frequency Domain)	66
29	Mu-Epsilon of Fiberglass (Time Domain)	67
30	Mu-Epsilon of LS-40 Absorber (Frequency Domain)	69
31	Mu-Epsilon of LS-40 Absorber (Time Domain)	70
32	Horn-Reflector Antenna Center Piece	74
33	Horn-Reflector Antenna Cover	75
34	Sample Holder Base Without Cover	76
35	Sample Holder Cover	77
36	Shorting Stub	78
37	Shorting Plug (A-Side) and Gage Block (B-Side)	79

## SECTION I

### INTRODUCTION

Over thirty years ago, extreme interest was shown in the design and construction of materials that absorb electromagnetic radiation. Recently, this interest has been quite intense, especially in the microwave and millimeter regions of the electromagnetic spectrum. Many new absorbers under development can function over wide frequency bands and in high temperature environments. Since in general the properties of absorbers are difficult to predict or calculate, their performance must be experimentally verified. The Avionics Laboratory (AFWAL/AA) has shown interest in absorber measurements since the early 1970's and knows full well the problems involved with measuring microwave absorbing materials.

In order to design or test any Radar Absorbing Material (RAM) it is essential to accurately know the electrical and magnetic properties of the material in question. These properties are characterized by the complex permittivity ( $\epsilon^*$ ) and permeability ( $\mu^*$ ) of the unknown material. For most real world absorbing materials,  $\mu$  and  $\epsilon$  are strong functions of frequency. Thus, if one wants to design a broadband absorber,  $\mu$  and  $\epsilon$  must be known at every design frequency. For a single sample, this might involve many measurements, which become tedious if performed one frequency at a time. Obviously, one might like to have some sort of automated measurement system, which can obtain ( $\epsilon^*$ ,  $\mu^*$ ) across the desired frequency range of interest. Can such a system be designed?

First of all, it is pertinent to discuss how to measure ( $\epsilon^*$ ,  $\mu^*$ ) of an unknown sample. It will be shown in Section II, that in order to determine  $\mu$  and  $\epsilon$  of a homogeneous sample of material, the scattering parameters of the unknown planar or coaxial sample must be obtained for the case of normally incident equiphase electromagnetic illumination. There are two widely known techniques by which scattering parameters can be obtained: the Time Domain and the Frequency Domain. Clearly, a choice must be made as to which approach will be used.

Several years ago, the Avionics Laboratory took delivery of a permittivity and permeability measurement system which obtained the scattering parameters through the Time Domain Method. Designed and built by the Sperry Rand Research Corporation (References 1-3), this system basically samples and digitizes the reflected and transmitted impulse response of a toroidal sample of absorber material residing in a coaxial airline. These sampled waveforms are subsequently Fourier Transformed and ratioed in order to determine the scattering parameters and hence the properties of  $\mu$  and  $\epsilon$ . Unfortunately, this time domain technique has two major restrictions which prevent the technique from being used at frequencies higher than 18 GHz. First, it is very difficult to sample waveforms with frequency content much above 18 GHz, due to limits in sampling oscilloscope technology. Secondly, it is difficult to build an accurate control system which can adjust quickly enough for slight timing shifts in the time domain measurement scans. Since the Air Force is ultimately interested in making measurements at frequencies above 18 GHz, clearly alternative measurement techniques must be investigated.

With the recent advent of stable computer-controlled, phase-locked microwave frequency synthesizers and network analyzers, it has now become practical to attempt scattering parameter measurements directly in the Frequency Domain. This immediately overcomes the upper frequency limit imposed on the Time Domain System, and has the added potential of obtaining a higher signal to noise ratio than was previously achieved in the Time Domain system. Thus, the main purpose of this thesis investigation is to design and build an automated measurement apparatus which can obtain  $\mu$  and  $\epsilon$  directly in the frequency domain with an accuracy of five to ten percent. It shall be demonstrated that such a measurement system can be constructed using a network analyzer and a dual horn reflector/sample holder reflectometer.

With these thoughts in mind, the organization of this thesis will be discussed. Section II, presents a generic problem of determining the material properties of  $\mu$  and  $\epsilon$  from the scattering parameters of

an infinite planar sample of material undergoing normally incident equiphase electromagnetic illumination. Some practical methods of approximating this infinite slab solution will be discussed, and a horn reflector/sample holder jig will be designed to implement the solution. Section 3, discusses how scattering parameters are made in practice, and the possible sources of error which can occur. It also proposes to use an accuracy enhancement model to attempt to reduce these potential measurement errors. Section 4, explains how to make single frequency and swept frequency ( $\mu^*$ ,  $\epsilon^*$ ) material measurements. In addition, Section 4 discusses the installation and testing of the Frequency Domain measurement system, and compares data obtained on the Frequency Domain System with data measured on the Time Domain System previously discussed. Finally, Section 5 makes some general conclusions and statements about future work in this area.

In addition to the main chapters of this thesis, there are three appendices. Appendix A provides complete engineering drawings of the antenna/sample holder arrangement designed in this thesis. Appendix B provides a computer listing of all calibration and control programs used in the Frequency Domain system, while Appendix C provides a detailed Standard Operating Procedure to correctly run the Frequency Domain System.

## SECTION II

THEORY BEHIND FREQUENCY DOMAIN MEASUREMENTS  
OF PERMITTIVITY AND PERMEABILITY

this chapter, the theory behind the Frequency Domain measurement will be developed. It is advantageous to begin with a very basic model and demonstrate how the scattering parameters are in terms of the incident, reflected and transmitted energy from the unknown material, which is assumed to have arbitrary  $\mu^*$  and  $\epsilon^*$ .

First of all, consider the situation pictured in Figure 1. An infinite unknown material with thickness  $d_1$  is illuminated by an equiphase magnetic wave at a single frequency. The incident wave will be denoted by  $\vec{a}_1$ , originating at the left. The reflected wave will be denoted by  $\vec{b}_1$ , while the wave transmitted through the sample and out to the right will be denoted by  $\vec{b}_3$ . Note that there is no incoming wave from the right, that is,  $\vec{a}_3=0$ . The quantities  $(\vec{a}_1, \vec{b}_1)$  are related to  $(\vec{a}_3 = 0, \vec{b}_3)$  by the wave transmission matrix as follows:

$$\begin{bmatrix} \vec{a}_1 \\ \vec{b}_1 \end{bmatrix} = \begin{bmatrix} a_{11} & a_{12} \\ a_{21} & a_{22} \end{bmatrix} \begin{bmatrix} \vec{a}_3 \\ \vec{b}_3 \end{bmatrix} \quad (1)$$

More Collin (Reference 4) and Nyquist (Reference 5) have both found the transmission matrix for a two-layered planar stratified media, as the case shown in Figure 1, if the air layer to the right is regarded as a second layer. In this case, the wave transmission matrix is as follows:

$$\begin{bmatrix} \vec{a}_1 \\ \vec{b}_1 \end{bmatrix} = \prod_{i=1}^2 \frac{1}{T_i} \begin{bmatrix} e^{j\theta_i} & R_i e^{-j\theta_i} \\ R_i e^{j\theta_i} & e^{-j\theta_i} \end{bmatrix} \begin{bmatrix} 0 \\ \vec{b}_3 \end{bmatrix} \quad (2)$$

$$\theta_i = K_i d_i \text{ with } K_i = \omega \sqrt{\mu_i^* \epsilon_i^*} \quad (3), (4)$$

Infinite Planar Slab of Unknown Material

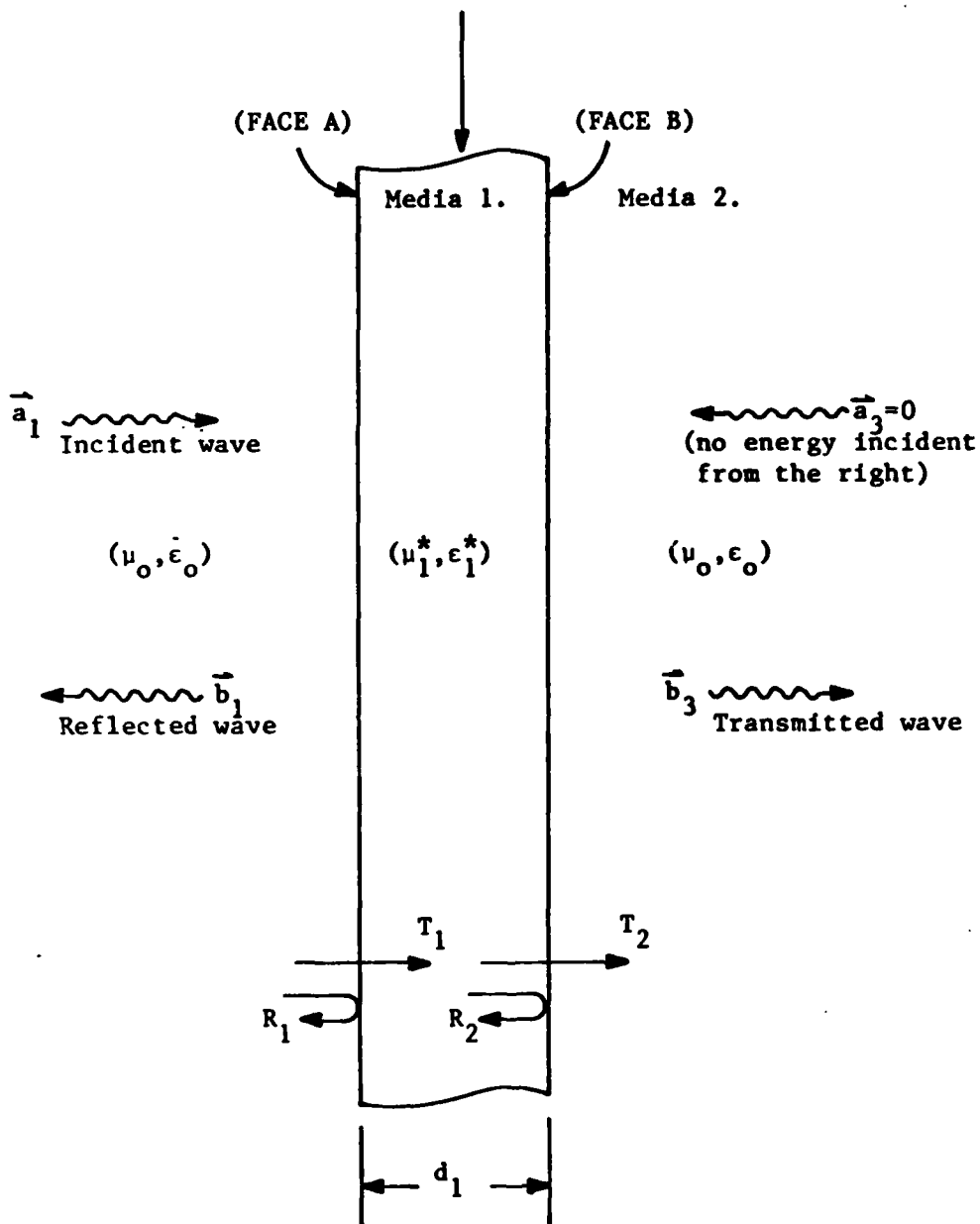


Figure 1. Geometry of Infinite Slab Problem

and  $(R_i, T_i)$  are the ordinary reflection and transmission coefficients at the front face of the individual layers respectively. In this problem, the layer of unknown material has the phase constant

$$\theta_1 = \omega \sqrt{\mu_1^* \epsilon_1^*} d_1 \quad (5)$$

Since the second "layer" of free space is infinite in extent, it is convenient to choose the phase reference of the absorber output at the right face, marked B, in Figure 1. In this case,

$$\theta_2 = 0 \quad (6)$$

Also, the reflection and transmission coefficients can be determined from the impedances of the media in the two layers. At the "front" face of the layer (marked A in Figure 1)  $R_1$  and  $T_1$  are given as follows:

$$R_1 = \frac{(Z_1 - Z_0)}{(Z_1 + Z_0)} = \Gamma_1 \quad (7)$$

$$T_1 = \frac{2Z_1}{(Z_0 + Z_1)} = 1 + \Gamma_1 \quad (8)$$

where

$$Z_1 = \sqrt{\frac{\mu_1^*}{\epsilon_1^*}} \quad (9)$$

and

$$Z_0 = \sqrt{\frac{\mu_0}{\epsilon_0}} \quad (10)$$

In a completely analogous manner, the reflection and transmission coefficients at the second face are

$$R_2 = \frac{(Z_0 - Z_1)}{(Z_0 + Z_1)} = -\Gamma_1 \quad (11)$$

$$T_2 = \frac{2Z_0}{(Z_0 + Z_1)} = 1 - \Gamma_1 \quad (12)$$



Substituting Equations 5, 6, 7, 8, 11 and 12 into Equation 2 will yield the following result.

$$\begin{bmatrix} \vec{a}_1 \\ \vec{b}_1 \end{bmatrix} = \frac{1}{(1 + \Gamma_1)(1 - \Gamma_1)} \begin{bmatrix} e^{j\theta_1} & \Gamma_1 e^{-j\theta_1} \\ \Gamma_1 e^{j\theta_1} & e^{-j\theta_1} \end{bmatrix} \begin{bmatrix} 1 & -\Gamma_1 \\ -\Gamma_1 & 1 \end{bmatrix} \begin{bmatrix} 0 \\ \vec{b}_3 \end{bmatrix} \quad (13)$$

Combining the two matrices into one gives a slightly more compact equation.

$$\begin{bmatrix} \vec{a}_1 \\ \vec{b}_1 \end{bmatrix} = \frac{1}{(1 - \Gamma_1^2)} \begin{bmatrix} e^{j\theta_1} - \Gamma_1^2 e^{-j\theta_1} & \Gamma_1 (e^{-j\theta_1} - e^{j\theta_1}) \\ \Gamma_1 (e^{j\theta_1} - e^{-j\theta_1}) & (e^{-j\theta_1} - \Gamma_1^2 e^{j\theta_1}) \end{bmatrix} \begin{bmatrix} 0 \\ \vec{b}_3 \end{bmatrix} \quad (14)$$

Next, it is necessary to change directions for a moment, and look at the definition of the well known scattering parameters. The scattering parameters relate the outgoing wave ( $\vec{b}_1, \vec{b}_3$ ) to the incoming waves ( $\vec{a}_1, \vec{a}_3 = 0$ ) in the following manner.

$$\begin{bmatrix} \vec{b}_1 \\ \vec{b}_3 \end{bmatrix} = \begin{bmatrix} S_{11} & S_{12} \\ S_{21} & S_{22} \end{bmatrix} \begin{bmatrix} \vec{a}_1 \\ 0 \end{bmatrix} \quad (15)$$

Obviously, the fact that  $a_3 = 0$  has already been utilized. From Equation 14

$$\vec{a}_1 = \frac{(e^{j\theta_1} - \Gamma_1^2 e^{-j\theta_1}) \vec{b}_3}{(1 - \Gamma_1^2)} \quad (16)$$

and

$$\vec{b}_1 = \frac{\Gamma_1 (e^{j\theta_1} - e^{-j\theta_1}) \vec{b}_3}{(1 - \Gamma_1^2)} \quad (17)$$

Taking ratios of Equation 17 to 16, and using the definition of  $S_{11}(\omega)$ , one obtains

$$S_{11}(\omega) \equiv \left. \frac{\vec{b}_1}{\vec{a}_1} \right|_{\vec{a}_3=0} = \frac{\Gamma_1 (1 - e^{-j2\theta_1})}{(1 - \Gamma_1^2 e^{-j2\theta_1})} \quad (18)$$

From Equation 16 and the definition of  $S_{21}$  one can also obtain

$$S_{21}(\omega) \equiv \left. \frac{\vec{b}_3}{\vec{a}_1} \right|_{\vec{a}_3=0} = \frac{(1 - \Gamma_1^2) e^{-j\theta_1}}{(1 - \Gamma_1^2 e^{-j2\theta_1})} \quad (19)$$

From the physical symmetry of the problem, and the assumption that the unknown sample is homogeneous, we know that:

$$S_{11}(\omega) = S_{22}(\omega) \quad (20)$$

and

$$S_{12}(\omega) = S_{21}(\omega) \quad (21)$$

Thus the scattering parameters given in Equations 18 and 19 are all well defined quantities related to the thickness of the sample and the intrinsic impedance given by Equation 9. Although the complex  $\mu$  and epsilon ( $\mu^*$ ,  $\epsilon^*$ ) are somewhat buried in the scattering parameters  $S_{11}(\omega)$ ,  $S_{21}(\omega)$ , there is a method of extracting them once the scattering parameters are known. This procedure will be shown next. First of all, to simplify the notation slightly, define the parameter  $z$  in the following manner:

$$z = e^{-j\theta_1} = e^{-j \frac{\omega}{c} \sqrt{\mu_r^* \epsilon_r^*} d_1} \quad (22)$$

where the constant  $c$  is the speed of light in free space. From Equation 18 and 19

$$S_{11}(\omega) = \frac{\Gamma_1 (1 - z^2)}{(1 - \Gamma_1^2 z^2)} \quad (23)$$

$$S_{21}(\omega) = \frac{(1 - \Gamma_1^2)Z}{(1 - \Gamma_1^2 Z^2)} \quad (24)$$

Also from Equations 7, 9, and 10, the reflection coefficient can be related to the relative ( $\mu_r^*$ ,  $\epsilon_r^*$ ) of the absorber layer.

$$\Gamma_1 = \frac{(Z_1 - Z_0)}{(Z_1 + Z_0)} = \frac{\sqrt{\frac{\mu_r^*}{\epsilon_r^*}} - 1}{\sqrt{\frac{\mu_r^*}{\epsilon_r^*}} + 1} \quad (25)$$

Suppose now that the scattering parameters  $S_{11}(\omega)$  and  $S_{21}(\omega)$  have been measured at a frequency of interest. Writing the sums and differences of the scattering parameters, one obtains

$$V_1 = S_{21}(\omega) + S_{11}(\omega) = \frac{(\Gamma_1 + Z)}{(1 + \Gamma_1 Z)} \quad (26)$$

and

$$V_2 = S_{21}(\omega) - S_{11}(\omega) = \frac{(Z - \Gamma_1)}{1 - \Gamma_1 Z} \quad (27)$$

Next, define the parameter "x" in the following manner.

$$x = \frac{(1 - V_1 V_2)}{(V_1 - V_2)} \quad (28)$$

After a considerable amount of algebra, one can show that

$$\Gamma_1 = x \pm \sqrt{x^2 - 1} \quad (29)$$

where the sign ambiguity is resolved by imposing the added constraint that

$$|\Gamma_1| \leq 1 \quad (30)$$

Rearranging Equation 26,

$$Z = \frac{(V_1 - \Gamma_1)}{(1 - V_1 \Gamma_1)} \quad (31)$$

we see that  $Z$  is determined since  $V_1$  and  $\Gamma_1$  are known from Equations 26 and 29. Recall that  $Z$  was defined by Equation 22. If the natural log of Equation 22 is taken, the resulting equation is

$$(\ln Z) = -j \frac{\omega}{c} \sqrt{\mu_r^* \epsilon_r^*} d_1 \quad (32)$$

At this point in the derivation, it is convenient to define two new constants,  $C_1'$  and  $C_2'$  as follows:

$$C_1' = \sqrt{\frac{\mu_r^*}{\epsilon_r^*}} \quad (33)$$

and

$$C_2' = \sqrt{\mu_r^* \epsilon_r^*} \quad (34)$$

From Equation 32, we see

$$C_2' = j \left( \frac{c}{\omega d_1} \ln Z \right) \quad (35)$$

From Equations 25 and 33, we obtain:

$$C_1' = \frac{(1 + \Gamma_1)}{(1 - \Gamma_1)} \quad (36)$$

which is another known quantity. Finally from Equations 33 and 34

$$\mu_r^* = C_1' C_2' \quad (37)$$

and

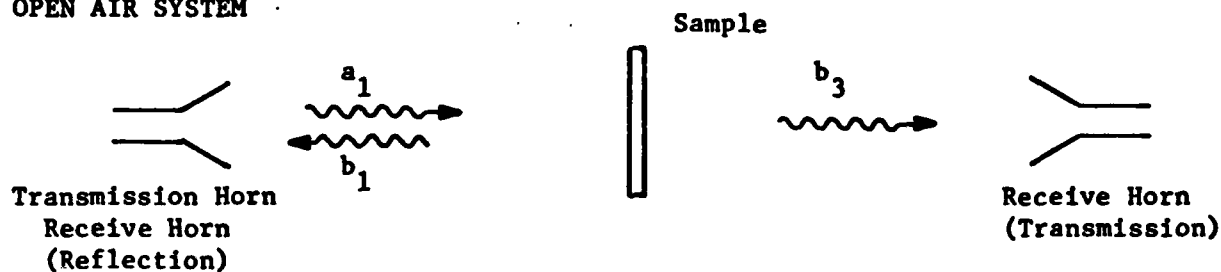
$$\epsilon_r^* = \frac{C_2'}{C_1'} \quad (38)$$

The conclusion of this derivation is that if the scattering parameters  $S_{11}(\omega)$  and  $S_{21}(\omega)$  are known at each frequency of interest, the complex permittivity and permeability can be calculated using the above complex arithmetic manipulations. Note that the subscript "r" in Equations 37 and 38 indicates "relative" to the free space permittivity and permeability ( $\epsilon_0$ ,  $\mu_0$ ).

With these thoughts in mind, it is necessary to visualize a method of implementing the solution to this rather abstract infinite slab model in a practical engineering ( $\mu, \epsilon$ ) measurement system. Before dwelling on how to obtain the scattering parameters, one must somehow find a method of realizing the initial assumptions of the previous theoretical discussion. As noted earlier, we assumed that an equiphase wave was normally incident on a slab of the unknown material. Can this condition be met in practice? Several free space and guided wave structures which closely approximate a planar phase wavefront normally incident on the unknown slab were investigated, and are shown in Figure 2. The advantages and disadvantages of each method will now be discussed in detail.

Under the first category of free space systems, a large (with respect to wavelength) flat plate of unknown material is placed in the far field of a pair of transmit-receive horn antennas. Since the sample is in the far field of the two antennas, the wavefront of the incident wave striking the sample should be nearly uniform in phase, as desired. Unfortunately, as desired. Unfortunately, since the sample is physically located a significant distance from the horns in order to meet the far field condition, a high percentage of the incident radiation is radiated in directions other than at the sample. Furthermore, if the materials are lossy, the reflections or transmissions through the samples may be over an order of magnitude down from the incident wave. Since the sample is located away from the antenna, these small reflected and transmitted signals are quite difficult to detect. The problem is especially acute on the reflected wave  $\vec{b}_1$ , since this set-up would use a single antenna to transmit and receive ( $\vec{a}_1, \vec{b}_1$ ), and the leakage of the incident signal  $\vec{a}_1$  might very well obscure the small reflected wave  $\vec{b}_1$ . Another major concern would be finding a method of accurately positioning a shorting plate and the sample plate in the exact same physical location, so that an accurate phase reference is established. Finally, in order to assure isolation from other equipment in the building, the test set-up would have to be located in an anechoic chamber, which incorporates an additional unnecessary expense. Hence, this particular approach was rejected.

OPEN AIR SYSTEM



CLOSED AIR SYSTEM

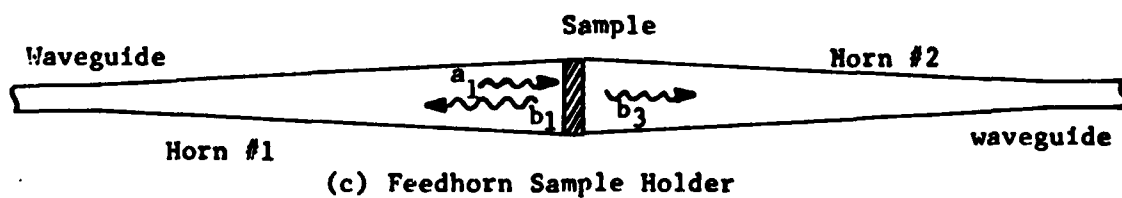
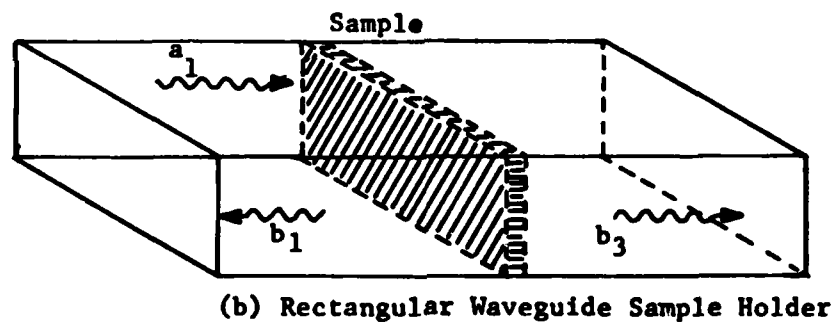
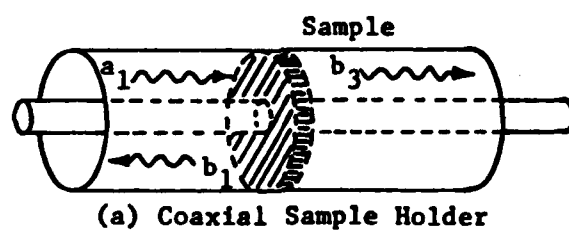


Figure 2. Potential Sample Holder Arrangements

The second category of closed waveguiding structures had several interesting sample holder configurations, three of which are shown in Figure 2. The first such scheme involved using a coaxial airline, with a toroidal shaped sample residing in the airline. This particular scheme is ideal from the standpoint that the electromagnetic wave striking the sample is a transverse electromagnetic wave (TEM), so the important equiphase condition is met. It must not be forgotten, however, that a coaxial line structure can support waveguide (TE or TM) modes. In order to avoid the moding problem, the proper size coaxial line must be chosen for the desired operating frequency range. For a measurement system operating between 12.4 - 18 GHz, a 3.5 mm coaxial line should be employed. For higher frequencies, the coaxial line would be even smaller in diameter. One of the major problems with a coaxial line sample holder is the actual machining of the samples. Many practical absorber materials are hard or brittle, and a 3.5 mm coaxial sample may be difficult to construct. The Time Domain measurement system discussed earlier uses a 14 mm coaxial line, and even at that size, samples are not easy to cut. The problem would become insurmountable at frequencies above 26 GHz, so this approach was also rejected from further consideration.

Another closed wave guiding system considered is the common rectangular waveguide. This particular scheme has the advantage of rectangular samples, which in principle would be easy to machine. The disadvantages included the fact that each particular waveguide band would require its own sample holder. In addition, the waveguide does not support a TEM wave, which would require some increased complexity in the signal processing. Since the Avionics Laboratory was not interested in building a sample holder at each operating frequency band, this option was also quickly discarded.

A third waveguiding structure considered blending the idea behind the free space system, and the wave guiding system. Basically, this approach would use two long (with respect to wavelength) horn antennas with small flare angles to obtain an electromagnetic wave in the aperture which meets the far field criteria ( $22.5^\circ$  phase variation in the aperture).

Such a sample holder configuration was first designed and tested by Aguirre (Reference 6). The operating frequency was 12.4 - 18.0 GHz, with an aperture size of 4.0" x .311". In order to meet the far field phase condition, each of the two horns were 4.5' in length. Adding all of the Ku waveguide plumbing necessary to complete the measurement set-up required a lot of additional undesirable waveguide components. In addition, the sample holder designed by Aguirre would not mate well with the two horn antennas. As a result of these problems, a significant amount of energy was attenuated in the measurement set-up, reducing the potential accuracy of his measurements. Overall, however, this particular illumination scheme had the potential of meeting all the desired conditions stated earlier. After careful consideration, however, this scheme was also rejected after yet another method presented itself as a more attractive alternative. This will be discussed next.

The final sample-holding system considered by the author involved using two waveguide-fed horn-reflector (References 7 and 8) antennas with a rectangular sample holder between the apertures of the two antennas. A sketch of the two antenna-sample holder system is shown in Figure 3. The basic idea involved using the horn-reflector antennas to convert the semi-spherical electromagnetic wavefront from the horn feed to a near uniform phase wavefront in the aperture. The rectangular sample holder nearly extends the aperture to provide a path for the equiphase wavefront from the antenna to the sample of material. A second horn-reflector antenna then converts the transmitted wave back to waveguide, and eventually to the waveguide detector. The total path length through the two horns and sample holder could be made considerably shorter than the set-up designed by Aguirre. Other advantages to this approach includes the fact that the two-horn reflector system could be well matched, with a fairly low voltage standing wave ratio (VSWR). The bandwidth of the horn-reflector antenna, another important consideration, can easily cover two waveguide bands. Hence a Ku band horn-reflector may be able to accommodate frequencies up through K-band (18.0 - 26.0), if the proper waveguide transitions are included in the test set-up.



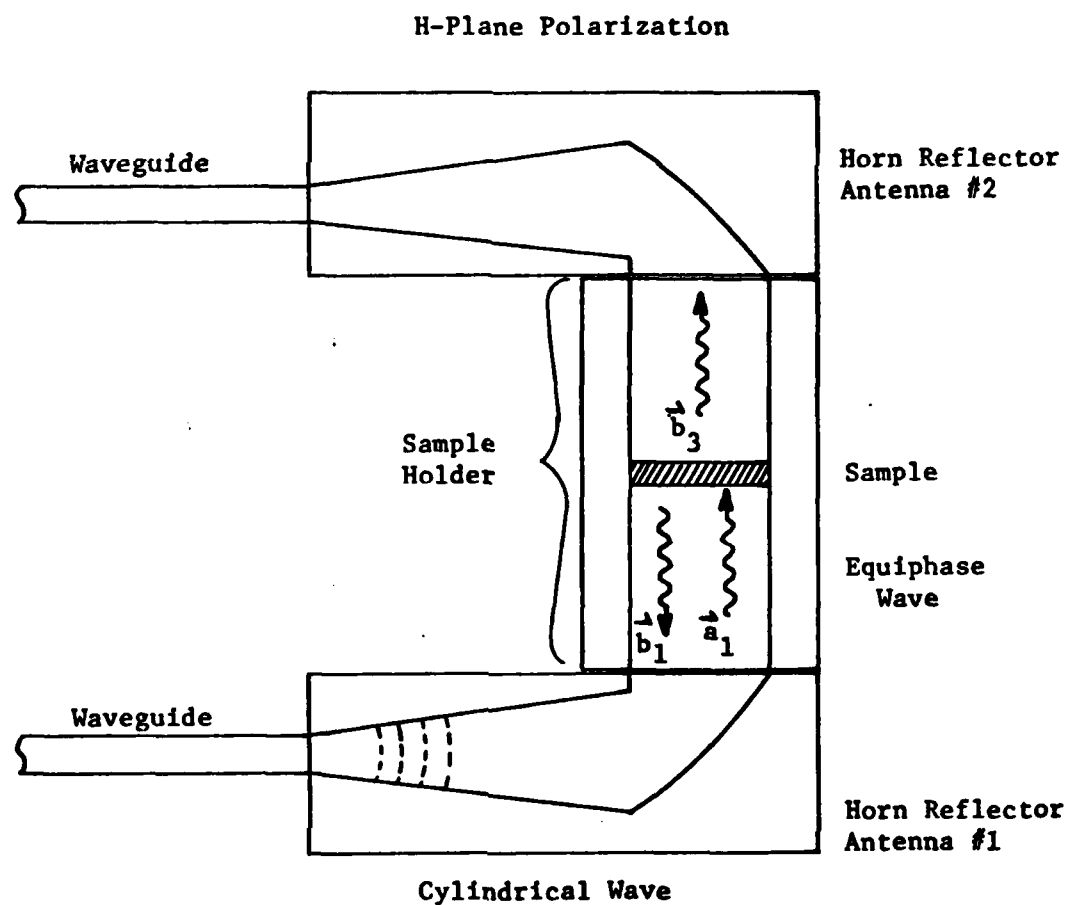


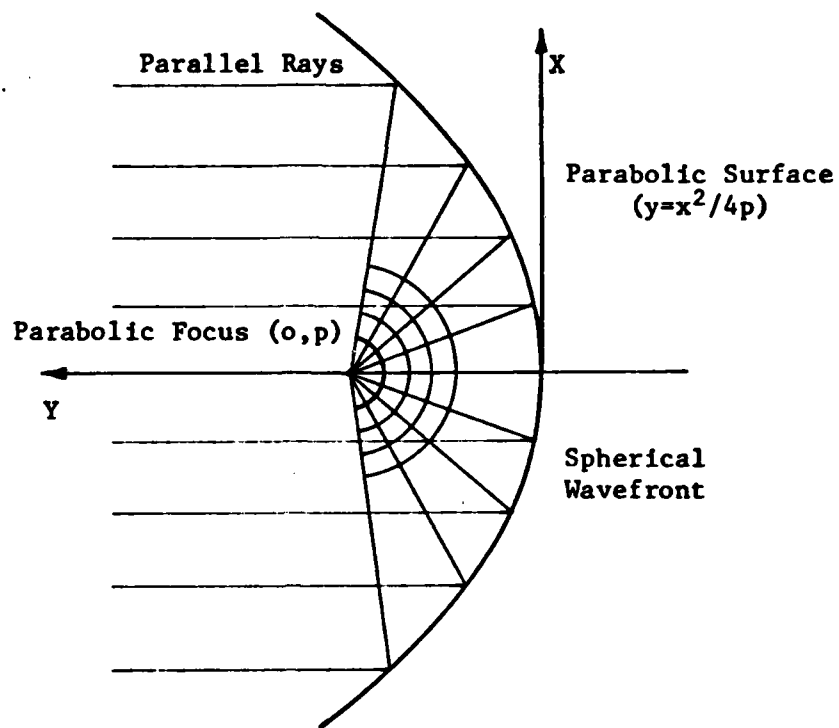
Figure 3. Dual Horn-Reflector Sample Holder Test Set-Up

Thus, with all of these advantages the horn-reflector sample holder system was chosen for use in the Frequency Domain measurement system.

Although higher order modes can exist in the rectangular sample holder and guide, these effects in the Ku-band should be small, if the discontinuities in the connections between the horn antennas and the sample holder are kept to a minimum. Field probes of the horn-reflector aperture using a tiny scattering sphere demonstrated a nearly  $TE_{10}$  amplitude profile. Since the mode structure in the rectangular sample should be the same as in the oversize guide, the energy in the sample holder should not in theory be converted to higher order modes. Nonetheless, in order to determine how serious the mode conversion problem is, comparisons will be made later in this thesis between Time Domain and Frequency Domain Measurement data.

The next important question involves what frequency band should be investigated first. Since the Avionics Laboratory currently has a synthesized frequency generator and network analyzer in-house that operates in the Ku frequency band (12.4 - 18.0) this frequency range was chosen for investigation in this thesis. An additional benefit for working in the Ku band is that the Avionics Laboratory Sperry measurement system can measure samples from 9.0 - 16.0 GHz, thus allowing some ability to cross check measurements between the Time Domain system and the Frequency Domain system.

After choosing the operating frequency range and radiating system to be used in the Frequency Domain measurement system, a discussion of the antenna theory and design must be undertaken. To understand the theory behind the horn-reflector antenna, consider a ray optics model shown in Figure 4. Suppose a point source of high frequency radiation is located at the parabola focus, as shown on Figure 4. The spherically diverging rays emerging from the focus will strike the surface of the parabolic reflector, and become parallel rays. When the antenna is acting in the receive mode, the incoming parallel rays will be focused at the parabola focus. The operation of a horn-reflector antenna is quite similar, and will be discussed next.



Geometry of Parabolic Reflection

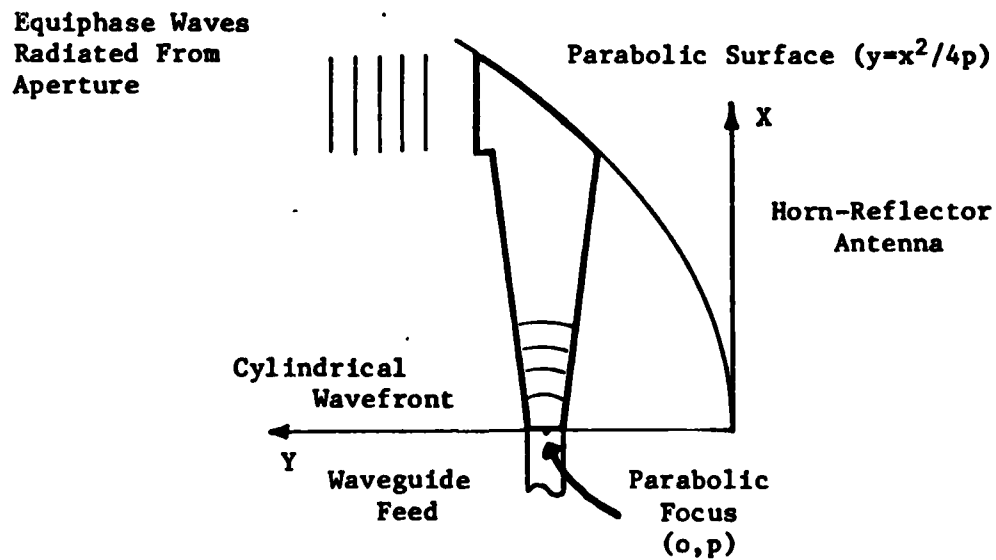


Figure 4. Geometry of Parabolic Reflector and Horn-Reflector Antennas

o in Figure 4, the focus of the parabola has now been located center of a Ku-band rectangular waveguide feed. The waves ng from the horn feed strike the section of the enclosed parabola, reflected out of the antenna structure in the direction of the erture. The wavefronts leaving the horn-reflector antenna are uiphase. The entire horn is enclosed, as shown, to prevent direct on from the waveguide feed point from reaching the antenna e.

should be mentioned at this point that horn-reflector antennas flared in both the E-plane and the H-plane. A classic example of e the hundreds of S-band horn-reflectors used in the Bell Telephone stance microwave network. Obviously, if the antenna in question ed in two planes, the resulting reflector surface is a section of oloid of revolution instead of a simple parabola. In the antenna ng system discussed here, the aperture height will correspond to the Ku-band waveguide feed height (.311") so that the horn flared in the H-plane, and the design problem is reduced to a one dimensional parabola.

igning a horn-reflector antenna flared in the H-plane is quite tforward, and simply requires careful sketches and precise y. To reduce the drudgery of drawings many potential antenna , a simple computer program was written to draw the proposed designs. Although this program will not be explored in detail, ly it would take a given waveguide feed dimension, desired aperture d focal length, and compute the horn feed flare angle and lly draw a two-dimensional picture of the antenna. For conve- the Avionics Laboratory desired rectangular samples as previously ed, so a desired aperture size of .311 x 2.0 inches was chosen. he waveguide feed dimensions were fixed (.622 x .311 inches), the riable was the focal length. Intuitively, the antenna shape vary considerably, as the focal length is varied. Figure 5 shows lf-scale drawings of three potential antenna designs. Notice that focus becomes smaller, the antenna became shorter in length and

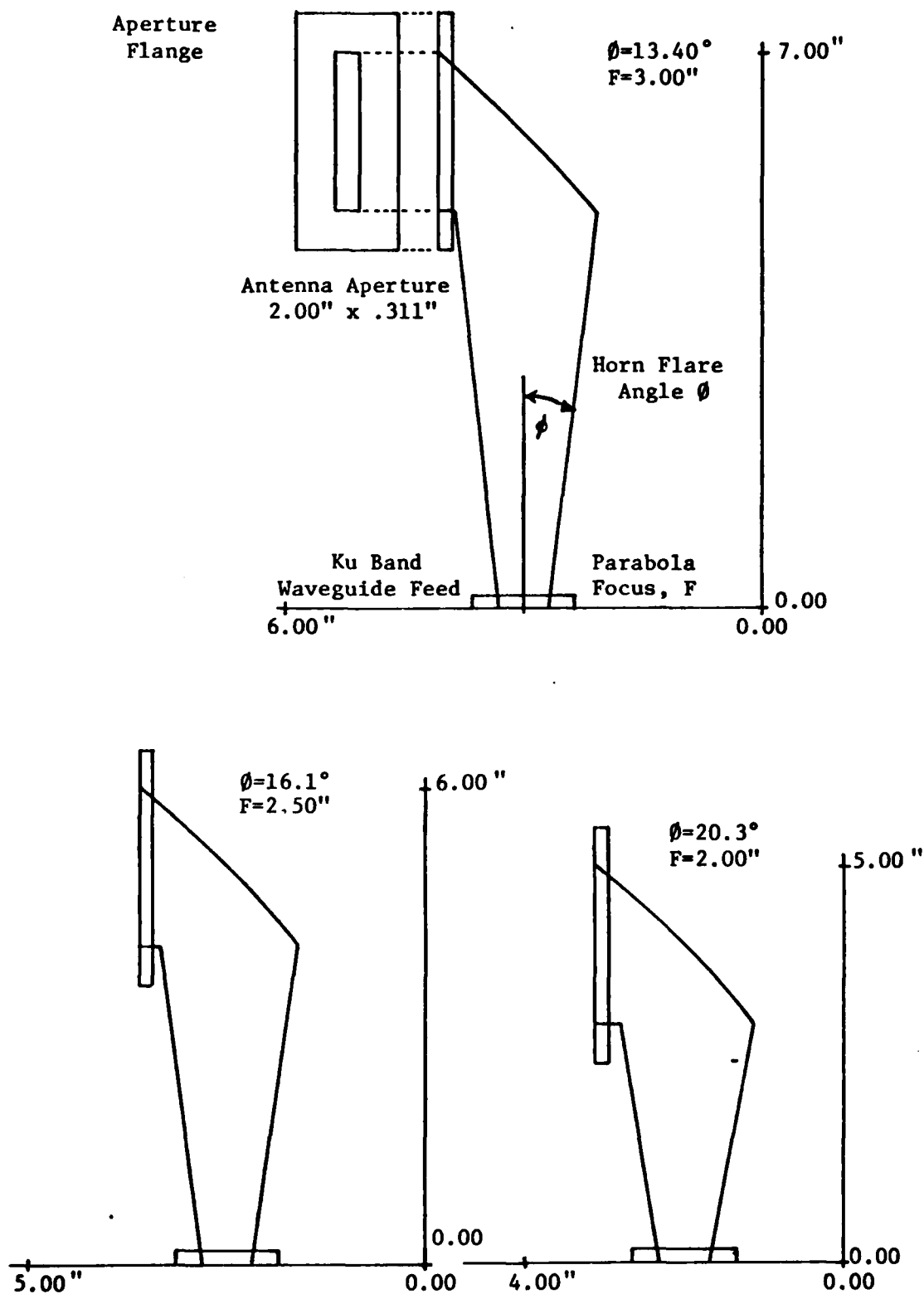


Figure 5. Variation of Horn-Reflector Shape with Focus Change

the parabolic reflector section became larger. After looking at dozens of potential designs, the top antenna of Figure 5 was selected. From a practical standpoint, it had a relatively small antenna flare angle, which should provide a low VSWR and a gently curved parabolic surface which could be easily machined. Hence, a set of engineering drawings were constructed based upon this design, and are shown in detail in Appendix A.

The next question involves the design of the sample holder itself. Basically, an extension of the .311 x 2.0 inch aperture is a desirable design, so long as a mechanism is included to align and support the two attached horn-reflector antennas. The final design consists of an oversized brass rectangular waveguide of dimension .311 by 2.0 inches with a removable cover to access the sample. A gage block is included to assist in precisely positioning the samples in the same location in the sample holder. A brass shorting block, also required for a phase reference in the background measurements, has also been included in the sample holder design. Finally, the sample holder and attaching horn-reflector antennas included guide pins and screw mounts to securely attach the entire structure together. Complete engineering drawings of the shorting block, gauge block, and sample holder are all included in Appendix A. Also, two photographs have been included in Figures 6 and 7 to show the dual horn-reflector/sample holder arrangement both with the top cover in place and with the cover removed and a sample positioned in the sample holder.

One final issue must be addressed before concluding this chapter. Since the sample holder is basically an oversized rectangular waveguide, how does one account for the fact that the wave in the aperture is not precisely an equiphase normally incident wave. In actuality it is well known that the incidence angle of a wave propagating down a rectangular waveguide varies as a function of frequency. Kraus and Carver (Reference 9) have derived this relationship, which is given below

$$\cos \theta_1 = \frac{\lambda_0}{\lambda_g} = \sqrt{1 - \left(\frac{f_{c10}}{f}\right)^2} \quad (39)$$



Figure 6. Photograph of Antenna/Sample Holder with Top Cover in Place



Figure 7. Photograph of Antenna/Sample Holder with Cover Removed and Teflon Sample in Place



where  $\lambda_g$  is the guide wavelength in the aperture guide, and  $f_{c10}$  is the  $TE_{10}$  cut-off frequency in the aperture guide. With an aperture width of 2 inches, the cut-off frequency for the  $TE_{10}$  mode is 2.95 GHz. Since the operating band for this system is 12.4 - 18.0 GHz, the incidence angle varies between 9 - 13 degrees, instead of zero as assumed. This slight difference in incidence angle makes the sample appear slightly electrically thinner than it actually is. In order to account for this minor difference, one must proceed back to Equation 5. By using the guide wavenumber  $k_g$  instead of the free space wavenumber  $k_0$  in Equation 5 as shown in Equation 40,

$$\theta_1 = k_g d_1 = k_0 d \sqrt{1 - \left(\frac{f_{c10}}{f}\right)^2} \quad (40)$$

We can account for the slight difference imposed by the non-normal incidence angle. In the actual mu-epsilon calculation, this would simply translate into a modification of Equation 32.

$$(\ln Z) = -j \frac{W}{c} \sqrt{\mu_r^* \epsilon_r^*} d_1 \sqrt{1 - \left(\frac{f_{c10}}{f}\right)^2} \quad (41)$$

All other aspects of the mu-epsilon calculation would remain the same.

In conclusion, this section investigated how the material constants of permittivity and permeability ( $\mu^*$ ,  $\epsilon^*$ ) of an unknown homogeneous planar sample of material can be derived if the scattering parameters of an infinite slab of the unknown material are known under equiphase electromagnetic illumination. Possible open and closed waveguide structures which could closely approximate the infinite slab model were investigated, and a dual horn-reflector sample holder system was selected for use in the Ku-band Frequency Domain measurement system. Finally, the actual design of a horn-reflector antenna and sample holder were completed.

Our basic model in this problem has assumed that the scattering parameters  $S_{11}(\omega)$  and  $S_{21}(\omega)$  can be measured given a certain type of enclosed radiating system. The next section will discuss in detail how the scattering parameters are measured using real world waveguide components and a microwave network analyzer.

### SECTION III

#### THEORETICAL AND PRACTICAL SCATTERING PARAMETER MEASUREMENT TECHNIQUES USING ACCURACY ENHANCEMENT MODELLING

In this section, a method is developed for measuring the scattering parameters of an arbitrary two-port microwave network using a network analyzer and waveguide directional couplers. An accuracy enhancement technique is developed to account for non-ideal waveguide components, adaptors, and detectors. Later, the dual horn-reflector/sample holder arrangement shall be included in the measurement set-up in order to demonstrate how to measure the scattering parameters of a planar sample of unknown material.

The first question to be answered in this section is how to measure the scattering parameters of an arbitrary Ku-band waveguide two-port network using ideal directional couplers and a network analyzer. Initially, it will be assumed that the waveguide components in the test measurement are without loss, and do not change any intrinsic characteristics (coupling, VSWR) as the frequency is varied. Under these assumptions, a potential frequency domain reflectometer is shown in Figure 8. The device under test (DUT) is a two-port waveguide network which can be any active or passive microwave device. A microwave oscillator is first tuned to the desired frequency. The incident wave  $\vec{a}_1$  propagates through an isolator down the waveguide to a 20 db directional coupler (coupler #1 in Figure 8). Ideally, one percent of the incident energy is coupled into the reference channel (Channel A) of the network analyzer. The remaining portion of the signal travels through the reversed directional coupler (#2) unaffected and enters the device under test. Part of the incident wave  $\vec{a}_1$  is reflected ( $\vec{b}_1$ ) and part is transmitted ( $\vec{b}_3$ ). The reflected wave  $\vec{b}_1$  is coupled through the reversed 20 db coupler (#2) and up to the switch position marked "REFL". Similarly, the transmitted wave  $\vec{b}_3$  is coupled through the third 20 db directional coupler and up to the switch position marked "TRANS".

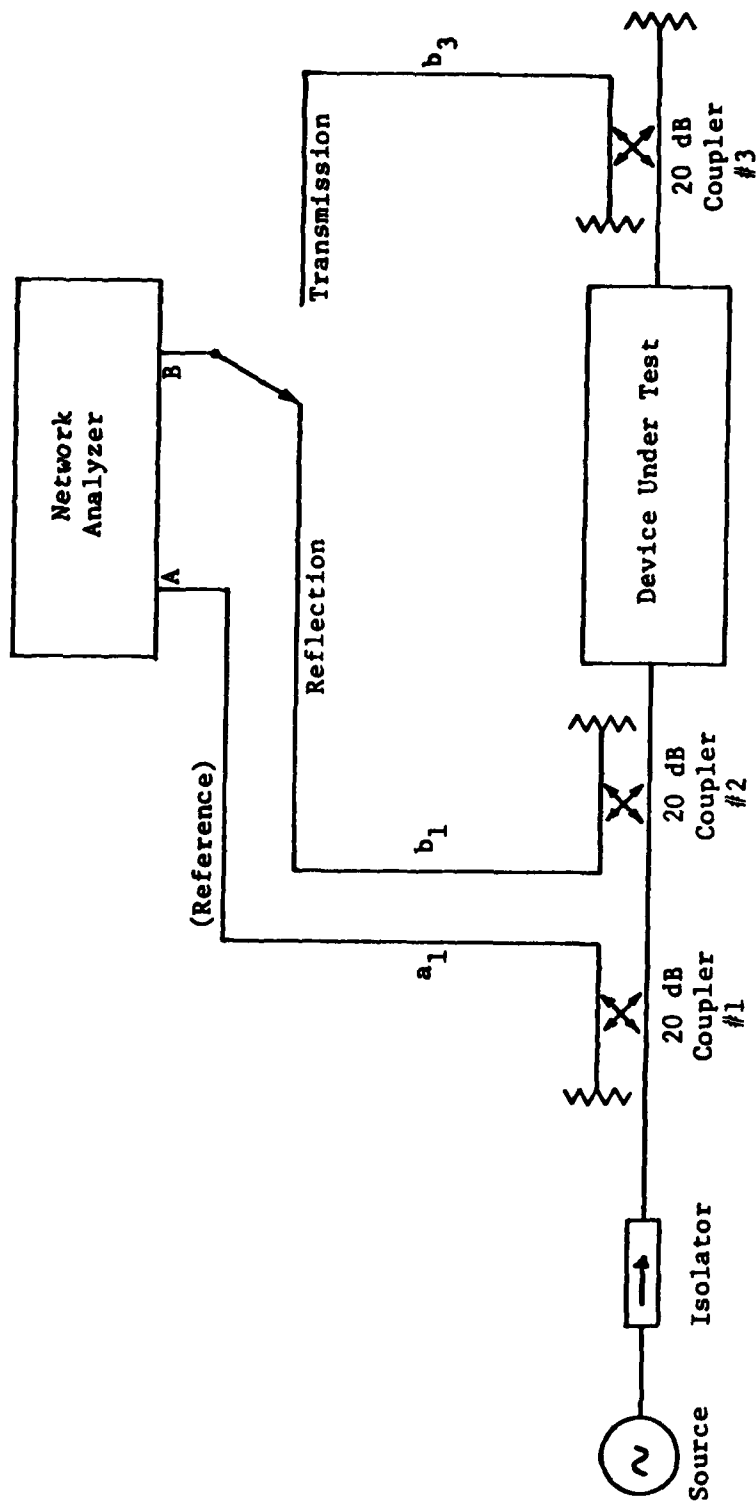


Figure 8. Idealized Scattering Parameter Reflectometer

The network analyzer performs the actual measurement at this point. When the reflection position is chosen, the network analyzer displays  $S_{11}(\omega)$  in amplitude and phase by internally taking the ratio of the Channel B input to the Channel A input.

$$S_{11}(\omega) = \frac{\vec{b}_1}{\vec{a}_1} = \frac{CHA \ B}{CHA \ A} = \text{Amp } e^{j \text{ Phase}} \quad (42)$$

Similarly, if one selects the transmission switch position, then the network analyzer displays the ratio of  $b_3$  to  $a_1$ , or  $S_{21}(\omega)$  as shown below.

$$S_{21}(\omega) = \frac{\vec{b}_3}{\vec{a}_1} = \frac{CHA \ B}{CHA \ A} = \text{Amp } e^{j \text{ Phase}} \quad (43)$$

Since all of the directional couplers are assumed to be ideal and equal, the measurements displayed on the network analyzer correspond in theory to the actual scattering parameters of the two-port device in question.

In the above discussion, all connections were assumed to be lossless, ideally coupled across the frequency band, with no discontinuities or impedance mismatches occurring in the measurement set-up. When using real world waveguide components and network analyzers, these particular assumptions are in general very poor, and can introduce a considerable amount of error in a practical measurement system Nicolson (Reference 10) demonstrated that for material measurements to be accurate to within five percent, the scattering parameters  $S_{11}(\omega)$  and  $S_{21}(\omega)$  must be known in amplitude and phase to within about three percent. Clearly since this is true, measurement errors must be reduced as much as possible. As a quick illustration of the magnitude of the problem, refer to the curve of Figure 9. This typical operating curve for a waveguide directional coupler is just one component of the test set-up. If this problem occurs with all directional couplers, how can the accuracy of the scattering parameter measurements be improved to an acceptable level?

Several major manufacturers of microwave measurement equipment have looked long and hard into this problem of accuracy enhancement techniques (References 11-13) and have developed proven methods of reducing

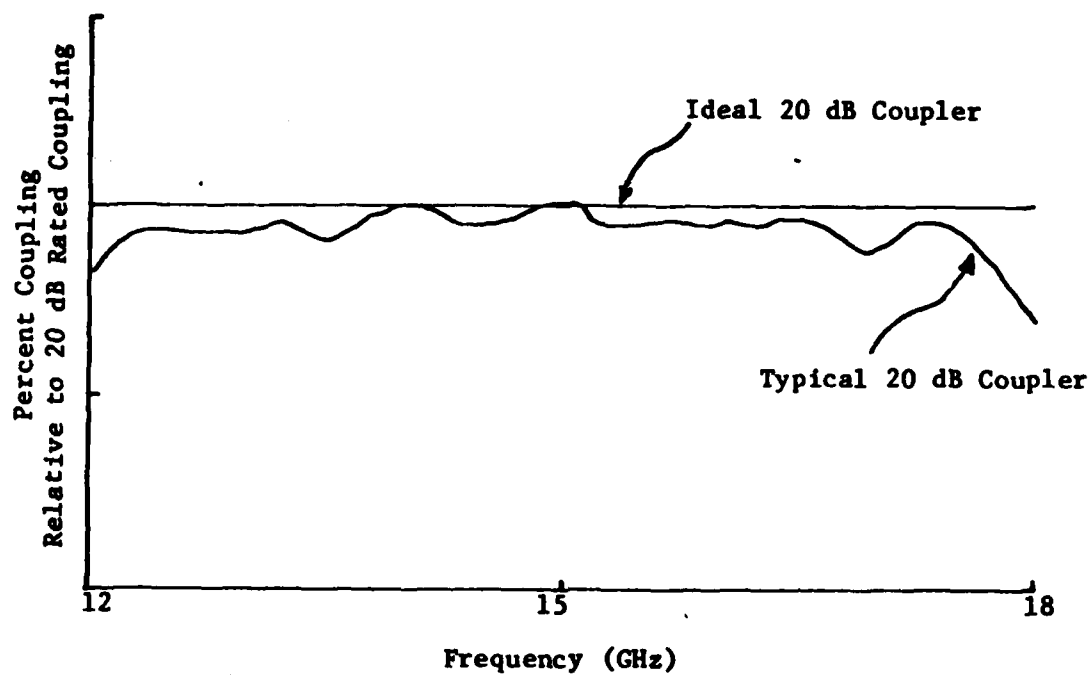


Figure 9. Frequency Dependence of a Typical 20dB Directional Coupler

measurement errors to acceptable levels. One such enhancement technique developed by Hewlett-Packard (Reference 14) employs an "error correcting" two-port circuit model which employs known standard microwave loads to accurately calibrate the model. This enhancement scheme shall be discussed next.

Before discussing a two-port accuracy enhancement model, it is desirable to first understand a one-port error correcting model, and to build on this knowledge when the two-port model is developed. Consider the non-ideal real world directional coupler/network analyzer reflectometer shown in Figure 10 (top), and replace it with a perfect reflectometer and a two-port error correction network also shown in Figure 10 (middle). The error correction network accounts for losses, minor mismatches due to the waveguide to coaxial line adaptors, and the differences in the receiver gains of the two-channel network analyzer. Notice in Figure 10, a difference exists between the measured reflection coefficient  $\Gamma_m$  and the actual reflection coefficient  $\Gamma_A$ . Looking at the flow diagram of Figure 10 (bottom) quickly allows one to write equations relating these two reflection coefficients.

$$\Gamma_m \equiv \frac{\vec{b}_0}{\vec{a}_0} = e_{00} + \frac{(e_{10}e_{01})}{1-e_{11}\Gamma_A} \quad (44)$$

The inverse relationship to Equation 44 is easily obtained.

$$\Gamma_m - e_{11}\Gamma_m\Gamma_A = e_{00} - e_{00}e_{11}\Gamma_A + e_{01}e_{10}\Gamma_A \quad (45)$$

$$\Gamma_A(e_{00}e_{11} - e_{11}\Gamma_m - e_{10}e_{01}) = e_{00} - \Gamma_m \quad (46)$$

$$\Gamma_A = \frac{\Gamma_m - e_{00}}{e_{11}(\Gamma_m - e_{00}) + e_{10}e_{01}} = \frac{\vec{b}_1}{\vec{a}_1} \quad (47)$$

Obviously, if the three error parameters  $e_{00}$ ,  $e_{11}$ , and  $e_{01}e_{10}$  are known then the measured reflection coefficient can be altered using Equation 47 to obtain the actual reflection coefficient  $\Gamma_A$ . Yet how are these error

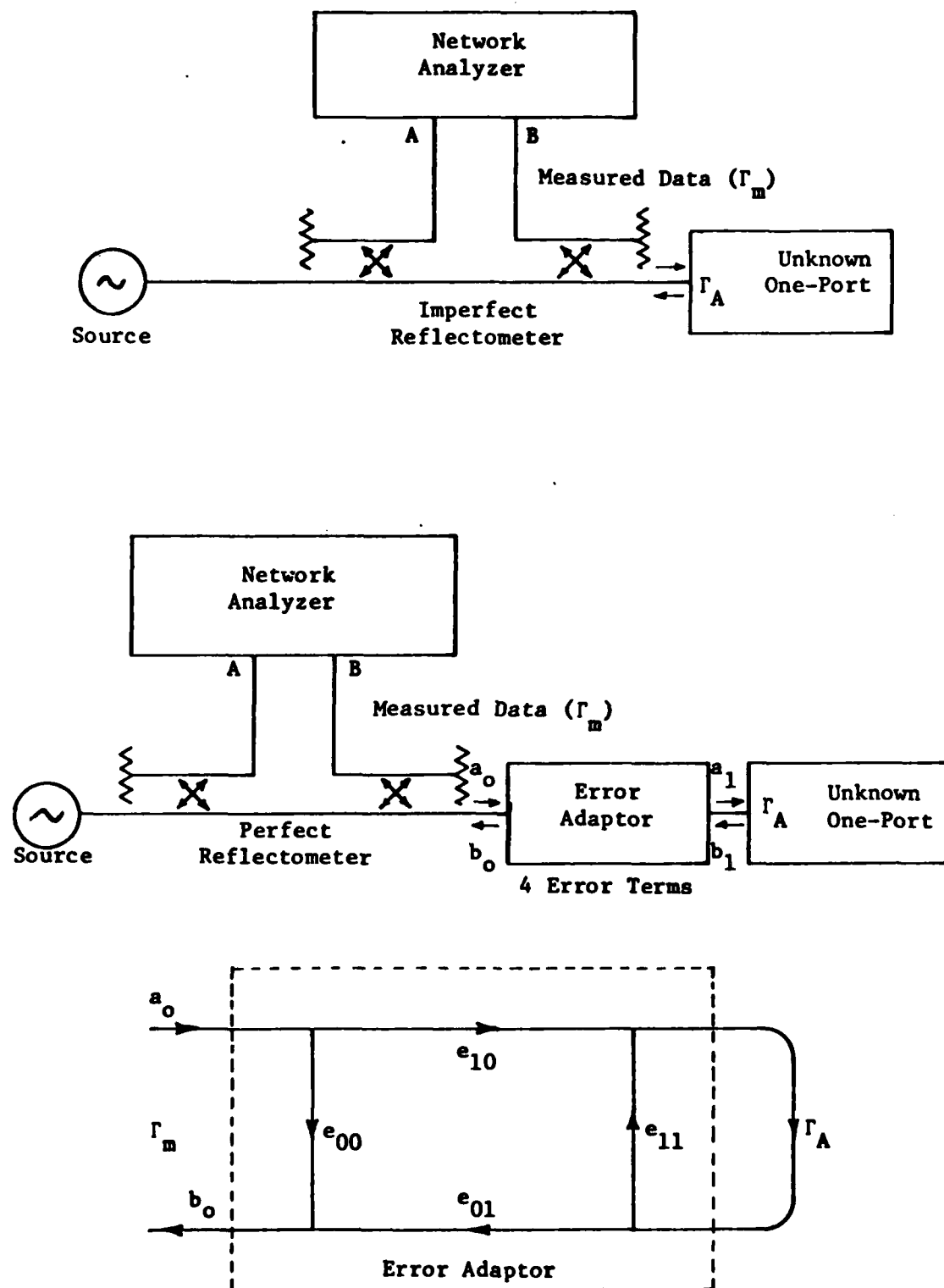


Figure 10. Modelling the Non-Ideal One-Port Reflectometer



terms determined? To answer this important question, write Equation 47 in a slightly different form.

$$a\Gamma_A + b - \Gamma_A\Gamma_{mc} = \Gamma_m \quad (48)$$

where

$$a = e_{10}e_{01} - e_{00}e_{11} \quad (49)$$

$$b = e_{00} \quad \text{and} \quad c = -e_{11} \quad (50,51)$$

Suppose now that one knows apriori the reflection coefficient from three precision standards. By using these three standards with known  $(\Gamma_{A1}, \Gamma_{A2}, \Gamma_{A3})$  and performing one measurement on each standard, three measured reflection coefficients  $(\Gamma_{m1}, \Gamma_{m2}, \Gamma_{m3})$  can be related to the known  $\Gamma_A$ 's, using Equation 48.

$$a\Gamma_{A1} + b - c\Gamma_{A1}\Gamma_{m1} = \Gamma_{m1} \quad (52)$$

$$a\Gamma_{A2} + b - c\Gamma_{A2}\Gamma_{m2} = \Gamma_{m2} \quad (53)$$

$$a\Gamma_{A3} + b - c\Gamma_{A3}\Gamma_{m3} = \Gamma_{m3} \quad (54)$$

Inverting these three equations and solving for a, b, and c yields the following equations:

$$c = \frac{[\Gamma_{m3} - \Gamma_{AeK1} - \Gamma_{m1} + \Gamma_{A1}K_1]}{[\Gamma_{A3}K_2 + \Gamma_{m1}\Gamma_{A1} - \Gamma_{A1}K_2 - \Gamma_{A3}\Gamma_{m3}]} \quad (55)$$

where

$$K_1 = \frac{(\Gamma_{m2} - \Gamma_{m1})}{(\Gamma_{A2} - \Gamma_{A1})} \quad (56)$$

and

$$K_2 = \frac{(\Gamma_{A2}\Gamma_{m2} - \Gamma_{A1}\Gamma_{m1})}{(\Gamma_{A2} - \Gamma_{A1})} \quad (57)$$

aining constants  $a$  and  $b$  are determined from

$$a = K_1 + cK_2 \quad (58)$$

$$b = \Gamma_{m1} + \Gamma_{m1}\Gamma_{A1}c - a\Gamma_{A1} \quad (59)$$

or terms  $e_{00}$ ,  $e_{11}$ ,  $e_{10}e_{01}$  are then determined from Equations 47-51.

$$e_{11} = -c = - \frac{[\Gamma_{m3} - \Gamma_{A3}K_1 - \Gamma_{m1} + \Gamma_{A1}K_1]}{[\Gamma_{A3}K_2 + \Gamma_{m1}\Gamma_{A1} - \Gamma_{A1}K_2 - \Gamma_{A3}\Gamma_{m3}]} \quad (60)$$

$$e_{00} = b = \Gamma_{m1} - \Gamma_{m1}\Gamma_{A1}e_{11} - \Gamma_{A1}(K_1 - e_{11}K_2) \quad (61)$$

$$e_{10}e_{01} = (K_1 - e_{11}K_2) + e_{00}e_{11} \quad (62)$$

be added that for ideal couplers and detectors,

$$e_{00} = e_{11} = 0 \quad (63)$$

$$e_{10}e_{01} = 1 \quad (64)$$

in Equation 47

$$\Gamma_A = \Gamma_m \mid \text{ideal} \quad (65)$$

next question to address is what known reflection coefficients used in the calibration procedure? When waveguide components are used, a convenient precision load is a sliding short. With a unity reflection coefficient magnitude, only the phase of the reflection coefficient is varied as the short position is changed. Hence, if three different short positions are chosen, and measurements are made at each short position, then the three equations in three complex unknowns (Equations 52-54) can be solved for the error parameters. For convenience, positions corresponding to 0.0, 1/3 guide wavelength, and 2/3 guide

wavelength will be selected. These three short positions correspond to the three independent known reflection coefficients

$$\Gamma_{A1} = | e^{j180^\circ} \quad (66)$$

$$\Gamma_{A2} = | e^{-j60^\circ} \quad (67)$$

and

$$\Gamma_{A3} = | e^{j45^\circ} \quad (68)$$

At this point, an important comment should be considered since the goal of this thesis involves developing an automated measurement system. Will this calibration procedure have to be undertaken every time the system is used? The answer to that question depends if the measurement set-up is altered. If the waveguide components used in the reflection side of the reflectometer are not physically changed from day to day, then the calibration procedure should not have to be repeated every day. Instead, the calibration data can be stored in a permanent file on the operating computer, where it will be available for use by the data processing software of the material measurement system.

Now that the one-port accuracy enhancement model is well understood, consider the two-port enhancement model. Figure 11 demonstrates how a non-ideal three-port reflectometer can be replaced by a perfect three-port reflectometer sandwiching a three-port error adaptor. The three-port error adaptor and the device under test (DUT) are shown in greater detail in Figure 12. Note that the actual device under test has the scattering matrix:

$$[S_A] = \begin{bmatrix} S_{11A} & S_{12A} \\ S_{21A} & S_{22A} \end{bmatrix} \quad (69)$$

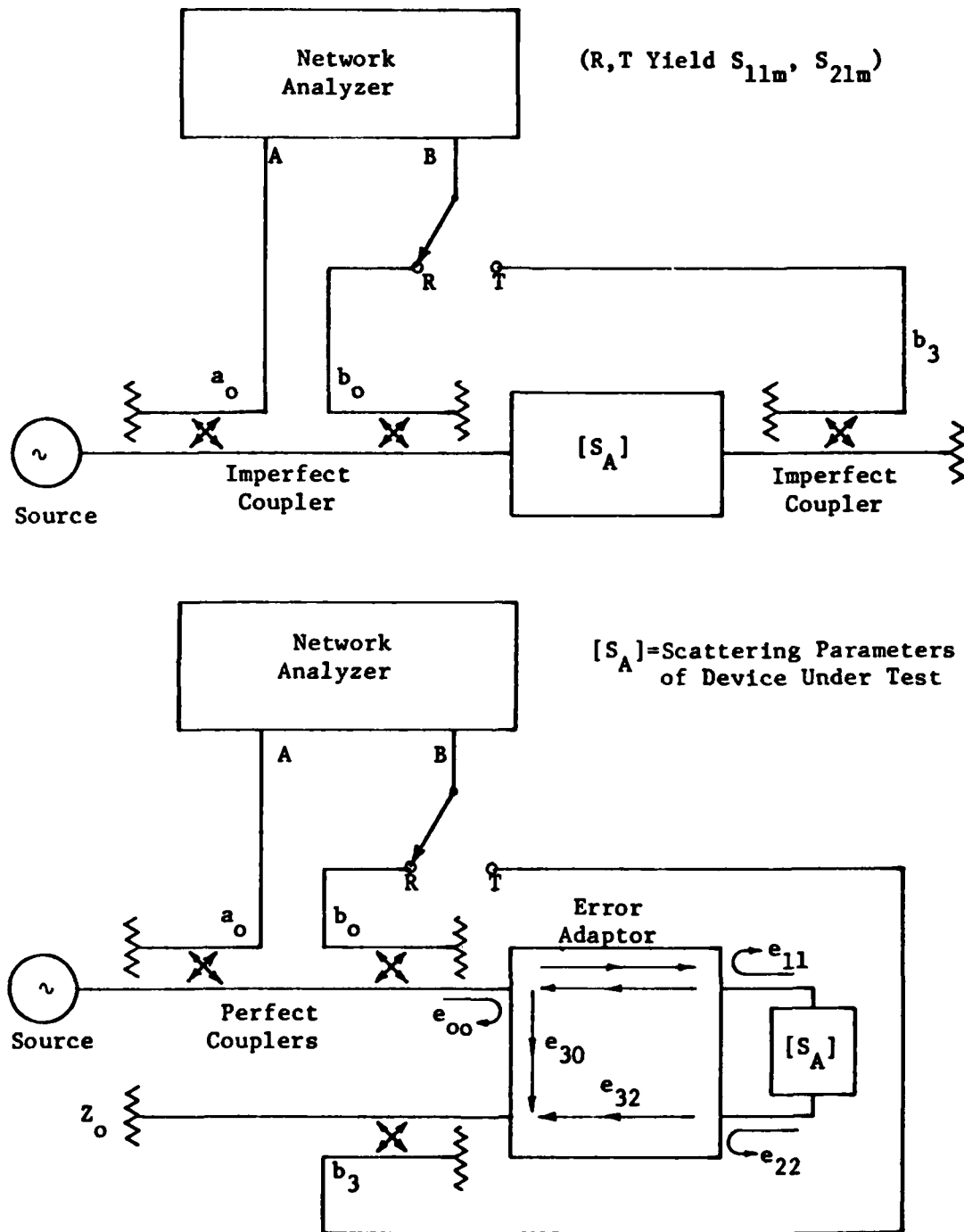


Figure 11. Modelling the Non-Ideal Two-Port Reflectometer

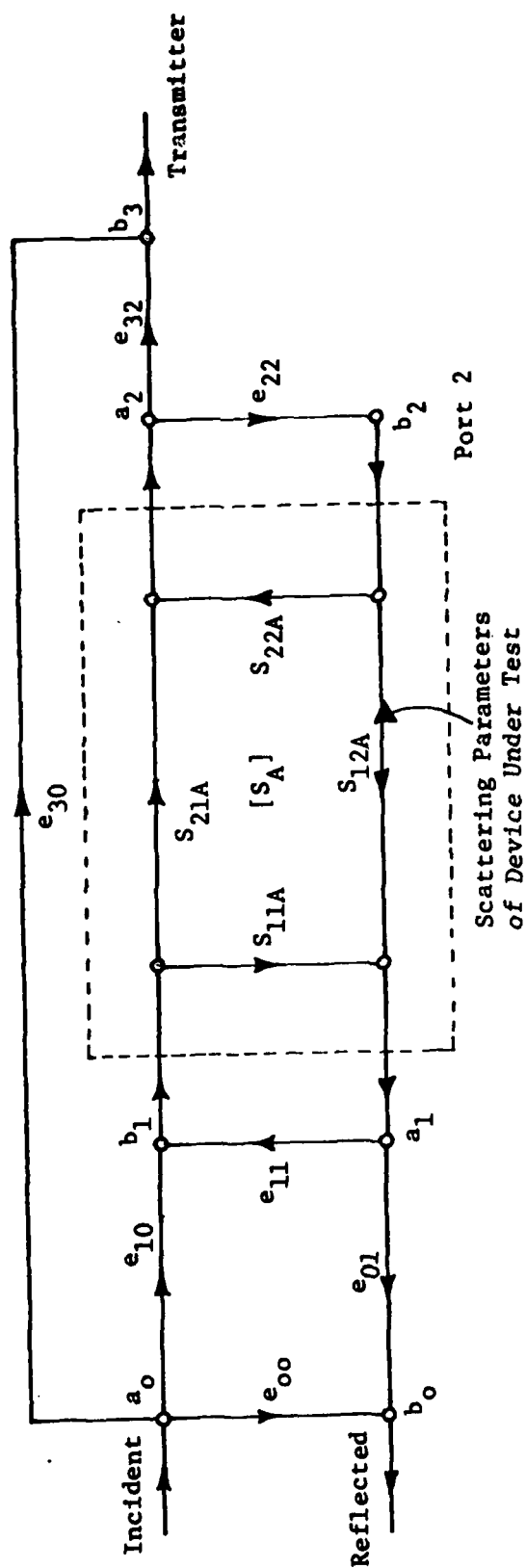


Figure 12. Flow Diagram for the Two-Port Error Model

The measured scattering parameters in terms of the actual scattering parameters can be obtained from the flow diagram of Figure 12 as follows:

$$S_{11m} = \frac{\vec{b}_0}{\vec{a}_0} = e_{00} + \frac{(e_{10}e_{01})[S_{11A} - e_{22}^{DET}(S_A)]}{1 - e_{11}S_{11A} - e_{22}S_{22A} + e_{11}e_{22}^{DET}[S_A]} \quad (70)$$

and

$$S_{21m} = \frac{\vec{b}_3}{\vec{a}_0} = e_{30} + \frac{e_{10}e_{32}S_{21A}}{1 - e_{11}S_{11A} - e_{22}S_{22A} + e_{11}e_{22}^{DET}[S_A]} \quad (71)$$

where

$$Det[S_A] = S_{11A}S_{22A} - S_{21A}S_{12A} \quad (72)$$

As pointed out in Equations 20 and 21, Equation 72 can be simplified for the case under investigation in this thesis.

$$Det[S_A] = S_{11A}^2 - S_{21A}^2 \quad (73)$$

Obtaining the inverse formulas for  $S_{11A}$  and  $S_{21A}$  in terms of  $S_{11m}$ ,  $S_{21m}$ , and the error parameters is difficult unless some minor approximations are made. In actual measurement systems, it has been found that

$$|e_{11}e_{22}| \ll 1 \quad (74)$$

(Typical data for  $e_{11}e_{22}$  was measured to be  $10^{-3}$  or less, which is small when compared to one in the complex plane). Thus in the denominator in Equations 70 and 71, let

$$e_{11}e_{22}(S_{11A}^2 - S_{21A}^2) \approx 0 \quad (75)$$

This simplification reduces the order of the resulting equation to a second order complex polynomial instead of a biquadratic polynomial.

Once this approximation is made, the following inverse relationships can be found after a great deal of algebra.

$$S_{11A} = \frac{-K_2 \pm \sqrt{\left(\frac{K_2}{K_1}\right)^2 - 4\left(\frac{K_3}{K_1}\right)}}{2} \quad (76)$$

with the root chosen such that

$$|S_{11A}| \leq 1 \quad (77)$$

and

$$K_1 = \left[ \frac{(e_{11} + e_{22})(S_{21m} - e_{30})}{e_{10}e_{32}} \right] e_{22} \quad (78)$$

$$K_2 = 2 \left[ \frac{S_{21m} - e_{30}}{e_{10}e_{32}} \right] (e_{11} + e_{22}) - \left[ 1 + \frac{(e_{11} + e_{22})(S_{11m} - e_{00})}{e_{10}e_{01}} \right] \quad (79)$$

and

$$K_3 = \frac{S_{11m} - e_{00}}{e_{10}e_{01}} - e_{22} \left( \frac{S_{21m} - e_{30}}{e_{10}e_{32}} \right) \quad (80)$$

The other inverse relationship is

$$S_{21A} = \left[ \frac{S_{21m} - e_{30}}{e_{10}e_{32}} \right] (1 - S_{11A} (e_{11} + e_{22})) \quad (81)$$

In order to compute the transmission error parameters ( $e_{32}e_{10}$ ,  $e_{30}$ ,  $e_{22}$ ) the reflection error parameters ( $e_{10}e_{01}$ ,  $e_{11}$ ,  $e_{00}$ ) must be known. Yet these reflect error parameters have been found from the previous one-port development. Hence the task is reduced to finding a calibration procedure which yields the transmission error parameters.

First, in order to determine  $e_{30}$  or the leakage from  $\vec{a}_0$  to  $\vec{b}_3$ , disconnect the device under test, and put matched loads on the two

directional couplers as shown in Figure 13. Under this test set-up,

$S_{12A}=S_{21A}=S_{11A}=S_{22A}=0$ ; hence from Equation 70

$$e_{30} = S_{21m} \left| \begin{array}{l} \text{Matched Load on Directional Couplers} \end{array} \right. \quad (82)$$

After numerous measurements in the Ku band reflectometer, it was found that for all frequencies of interest  $e_{30} = 0$ .

Next, connect directional couplers two and three to the horn-reflector/sample holder input and output ports as shown in Figure 14. Place the top cover on the empty sample holder. In this case

$$S_{12A} = S_{21A} = 1 \quad (83)$$

and

$$S_{11A} = S_{22A} = 0 \quad (84)$$

Then from Figure 14

$$S'_{11m} \left| \begin{array}{l} \text{empty sample} \\ \text{holder} \end{array} \right. = \frac{\vec{b}_0}{\vec{a}_0} = e_{00} + \frac{(e_{10}e_{01}e_{22})}{1 - e_{11}e_{22}} \quad (85)$$

Since  $(e_{00}, e_{11}, e_{10}e_{01})$  are known from the one port calibration procedure, Equation 85 can be solved for  $e_{22}$ .

$$e_{22} = \frac{S'_{11m} - e_{00}}{e_{01}e_{10} + S'_{11m} - e_{00}} \quad (86)$$

Leaving the test set-up unaltered, the transmission scattering parameter is measured. Since  $e_{30} = 0$ , this will yield an equation for the final



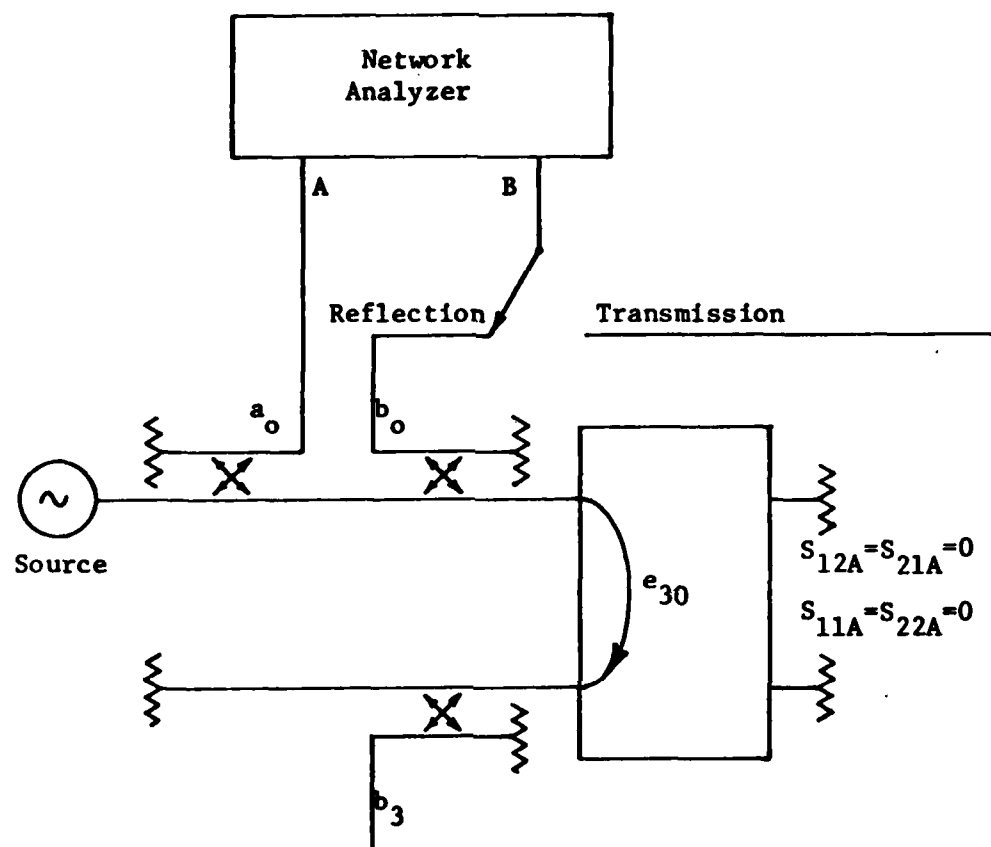


Figure 13. Measuring the Leakage Error Term  $e_{30}$

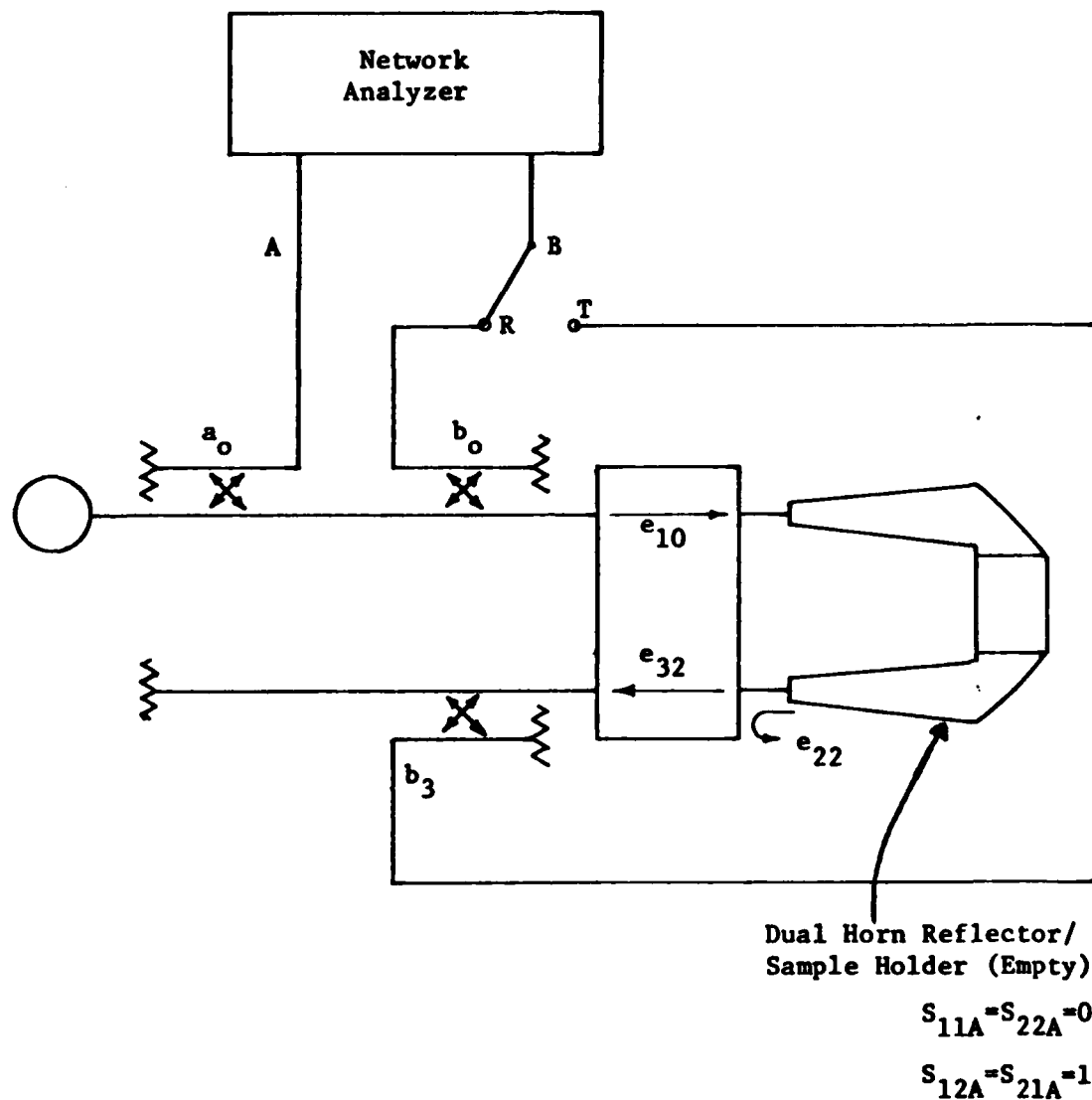


Figure 14. Measurement Set-up for the Transmission Error Parameters  $e_{22}$  and  $e_{10}e_{32}$

transmit error parameter  $e_{10}e_{32}$ . From Figure 14, and the signal flow diagram for this problem, one can obtain

$$S'_{21m} \left| \begin{array}{l} \text{empty sample} \\ \text{holder} \end{array} \right. = \frac{\vec{b}_3}{\vec{a}_0} = \frac{e_{10}e_{32}}{1 - e_{11}e_{22}} \quad (87)$$

Inverting Equation 87 yields after rearrangement

$$(e_{10}e_{32}) = S'_{21m} (1 - e_{11}e_{22}) \quad (88)$$

It should be mentioned that for an ideal three-port reflectometer,  $e_{22}=e_{30}=e_{11}=e_{22}=0$  and  $e_{10}e_{32}=e_{01}e_{10}=1$  causing Equations 70 and 71 to reduce to  $S_{11m}=S_{11A}$ ,  $S_{21m}=S_{21A} \left| \begin{array}{l} \text{ideal reflectometer} \end{array} \right.$ . At this point in

the error analysis, all six error parameters are known. Any sample can now be placed in the sample holder, and the scattering parameters measured ( $S_{11m}$ ,  $S_{21m}$ ), then corrected ( $S_{11A}$ ,  $S_{21A}$ ) using Equations 76 and 81. Yet, this is not the end of the calibration procedure. To fully account for the precise positioning of the unknown sample in the sample holder, one final step must be included. This aspect of the problem is discussed next.

Before the unknown sample can be inserted in the sample holder, it is necessary to insert a rectangular shorting block with its front face in the exact position to be occupied by the unknown sample. This precise positioning is required in order to get an accurate phase reference, which is needed to precisely determine the physical location of the sample in the sample holder. A separate gage block has been constructed in order to assist in positioning the short and sample. With the short in its proper position, the top is replaced on the sample holder, and the scattering parameters are measured ( $S_{11m}$ ,  $S_{21m}$ ) then corrected ( $S_{11A}$ ,  $S_{21A}$ ). As expected,  $S_{21A}$  is so close to zero that it is completely ignored. With this in mind, define a new symbol as follows:

$$S_{11SH}(\omega) = S_{11A}(\omega) \left| \begin{array}{l} \text{shorting plug in sample holder} \end{array} \right. \quad (89)$$

If the brass horn antennas were lossless, the reflection coefficient due to the shorting block would be very close to one in magnitude. Attenuation due to brass wall loss between the horn waveguide feed and the short position in the waveguide causes the magnitude of the reflection coefficient of the brass short to drop down to a magnitude of .88 or greater. The magnitude drop does not present a problem, however, since this can be easily normalized out of the sample measurements. The important item in the measurement is the phase angle of the short measurement, which is used to precisely determine the sample position in the sample holder.

Next, remove the short in the sample holder and place the unknown sample in the sample holder once again using the gage block to carefully position the sample. Replace the cover and measure ( $S_{11m}$ ,  $S_{21m}$ ) using the network analyzer. Correct these measurements using Equations 76 and 81 to obtain  $S_{11A}$ ,  $S_{21A}$ . The actual scattering parameters of the unknown planar sample of material are then found from the following equations:

$$S_{11}(\omega) = \frac{S_{11A}(\omega)}{S_{11SH}(\omega)} \quad (90)$$

$$S_{21}(\omega) = S_{21A}(\omega) \quad (91)$$

The complex constants ( $\mu_r^*$ ,  $\epsilon_r^*$ ) can then be determined using Equations 26-41 as developed in the second section. This completes the theory behind making corrected material measurements at a single frequency using the dual horn-reflector/sample holder Frequency Domain Reflectometer.

In conclusion, this chapter has investigated how ideal scattering parameter measurements are made. It also discussed in detail some of the inaccuracies that can enter into typical waveguide scattering parameter measurements and developed a two-port error model which will substantially increase the accuracy of the overall scattering parameter measurement set-up. A procedure was developed for calibrating

the error model, complete with flow graphs and precise instructions. Finally, a proposed measurement set-up was presented which can measure the scattering parameters of a planar sample of unknown material using the dual horn reflector/sample holder arrangement designed in Section II.

#### SECTION IV

##### AUTOMATED FREQUENCY DOMAIN MATERIAL MEASUREMENT SYSTEM

In the preceding section a method was developed for measuring the scattering parameters of an unknown planar sample of material using a network analyzer, a reflectometer, and a two-port dual horn-reflector/sample holder. A comprehensive three-port error model was developed to enhance the accuracy of the scattering parameter measurement set-up, and detailed procedures were outlined to calibrate the error model completely. All of the above items were developed for a single fixed frequency measurement set-up. The main purpose of the section is to present a final design for an automated stepped Frequency Domain measurement system, and update the operating procedures to reflect the hardware additions. Finally, a detailed discussion on the installation and experimental evaluation of this automated test set-up will be undertaken.

The design for an automated stepped Frequency Domain measurement system is shown in Figure 15, with a photograph included in Figure 16. Before exploring the detailed measurement procedures, take a close look at some of the new additions to the measurement set-up. Note that a Hewlett-Packard 21MX minicomputer with a cartridge disk storage system has been added to control and process the stepped frequency measurements. The minicomputer can set the operating frequency of the synthesized microwave frequency oscillator, and control a coaxial single pole double throw switch which selects the scattering parameter ( $s_{11}$  or  $S_{21}$ ) to be measured by the network analyzer. The HP 21MX also has an analog to digital converter which allows the amplitude and phase data measured by the network analyzer to be read and stored by the computer. Further note that an additional 3 db directional coupler has been added to the set-up in order to improve the isolation between the reflected signal  $\vec{b}_1$  and the frequency source. This extra isolation arm also assures that the reference signal  $\vec{a}_1$  is maintained at a constant level. Except for the additions explained above, this set-up is still essentially the three port reflectometer shown in Figure 11. Therefore, all the error modelling techniques previously discussed still apply to this test set-up.

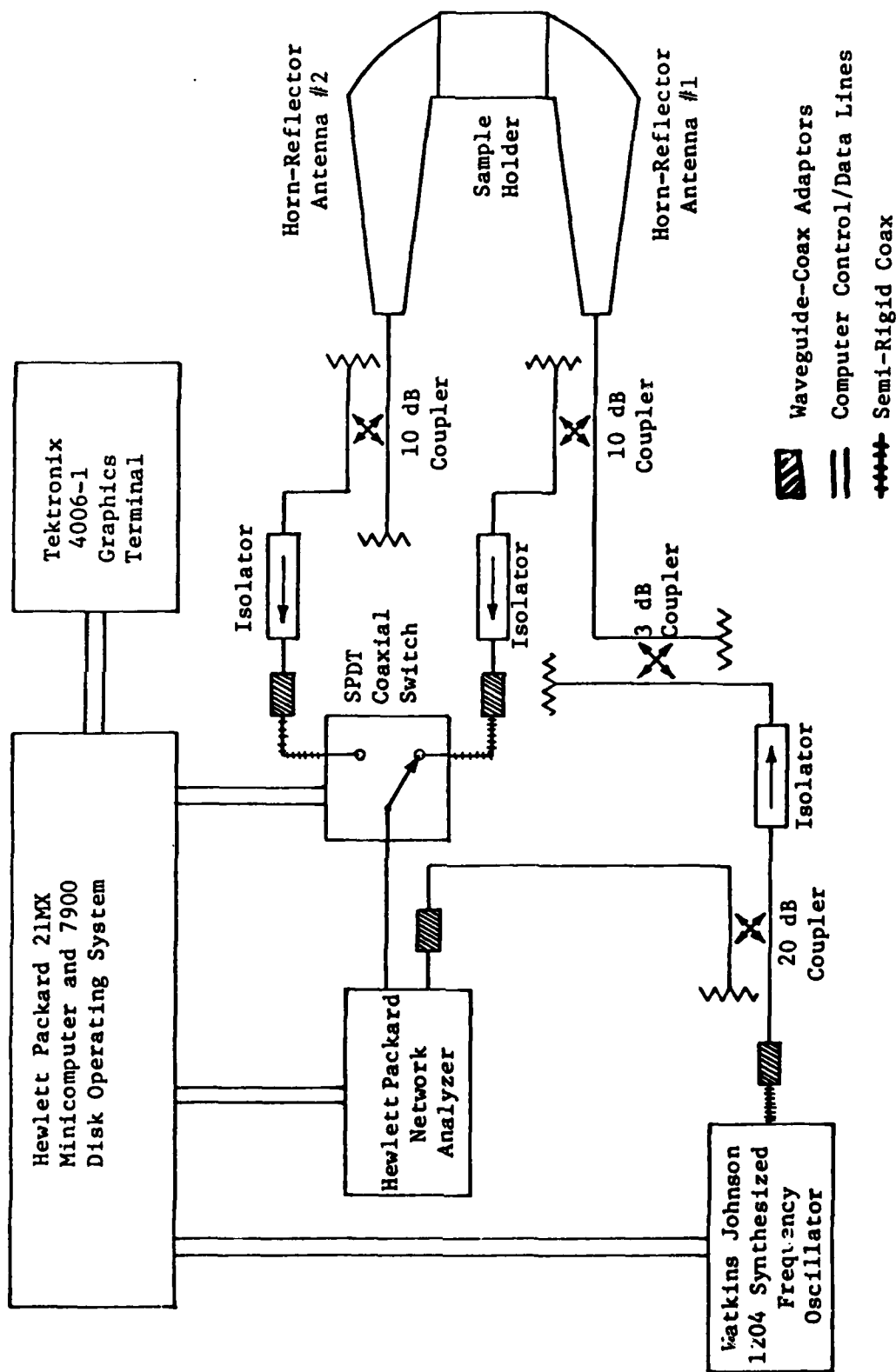


Figure 15. Finalized Frequency Domain Material Measurement System

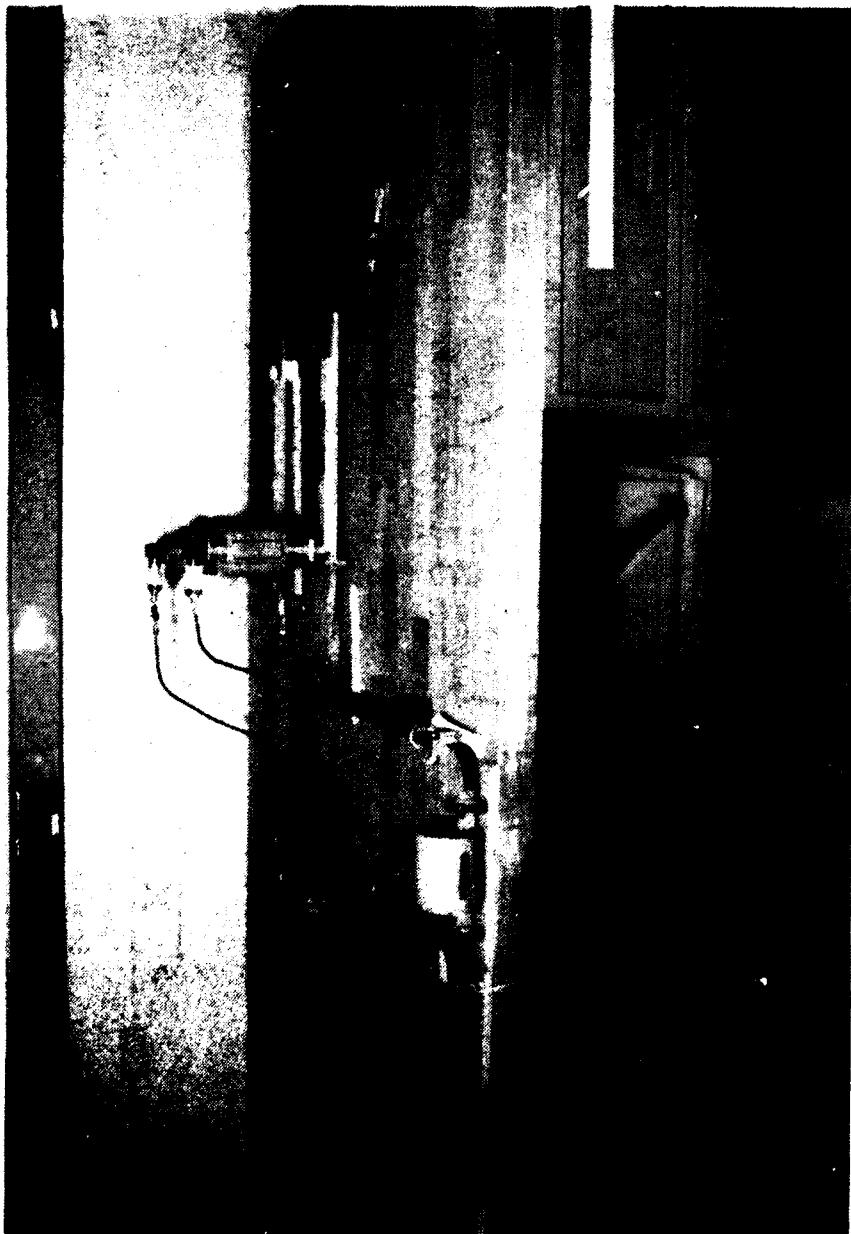


Figure 16. Photograph of Dual Horn-Reflector/Sample Holder Reflectometer



Legend

1. Frequency Input
2. 20 dB Directional Coupler #1
3. Isolator
4. 3 db Directional Coupler
5. Reversed 10 db Directional Coupler #2
6. Dual Horn-Reflector/Sample Holder
7. 10 db Directional Coupler #3
8. Path for Reflect Signal  $\vec{b}_1$
9. Path for Transmit Signal  $\vec{b}_3$
10. Computer Activated SPDT Coaxial Switch
11. Receiver Head for Network Analyzer
12. Path for Reference Signal  $a_1$
13. Precision Sliding Short Used for Reflect Error Calibration

Legend For Figure 16

The next question to address is how to calibrate the automated Frequency Domain Measurement System. As mentioned in Section III, all of the five major error parameters ( $e_{00}$ ,  $e_{11}$ ,  $e_{22}$ ,  $e_{10}e_{01}$ ,  $e_{10}e_{32}$ ) must be obtained first. Before the transmit error parameters ( $e_{22}$  and  $e_{10}e_{32}$ ) are determined, the reflect error parameters ( $e_{11}$ ,  $e_{00}$ ,  $e_{10}e_{01}$ ) must be found for every operating frequency at which material measurements are desired.

In order to measure and store the reflect error parameters, a separate calibration program (CALNA) was written. Basically, this program will step through the three shorting stub position measurements discussed in Section III at every operating frequency. After the three measured reflection coefficients ( $\Gamma_{m1}$ ,  $\Gamma_{m2}$ ,  $\Gamma_{m3}$ ) are found at each frequency, the reflect error parameters  $e_{00}$ ,  $e_{11}$ ,  $e_{10}e_{01}$  are computed using Equations 56-62 and stored in a permanent disk file on the minicomputer. Although it is not required to repeat this calibration procedure as long as the physical components of the reflectometer are not changed, it will be recommended by the author to update the error parameters periodically. A generalized flowchart of program CALNA is shown in Figure 17, and complete computer listings may be found in Appendix B.

After the calibration program is completed, the material measurement software can be initiated. This particular computer program (FDMSP) controls all aspects of the Frequency Domain Measurement System. The overall program organization of FDMSP is shown in flowchart form in Figure 18. Basically, the program performs three general functions. First of all, it takes a background scan of the empty sample holder, measuring  $S_{11m}$  and  $S_{21m}$ . By recalling the reflect error parameters ( $e_{00}$ ,  $e_{11}$ ,  $e_{10}e_{01}$ ) from the permanent disk file #EMAT1, the transmit error parameters ( $e_{22}$ ,  $e_{32}e_{10}$ ) are calculated using Equations 86 and 88. The second program subsection takes a reflection measurement of the shorting plug in order to establish a phase reference point for the exact sample position in the sample holder. Lastly, the third subsection takes reflection and transmission measurements ( $S_{11A}$ ,  $S_{21A}$ ) at each design frequency of the unknown sample of material, finally computing and plotting the permittivity and permeability as a function of frequency.

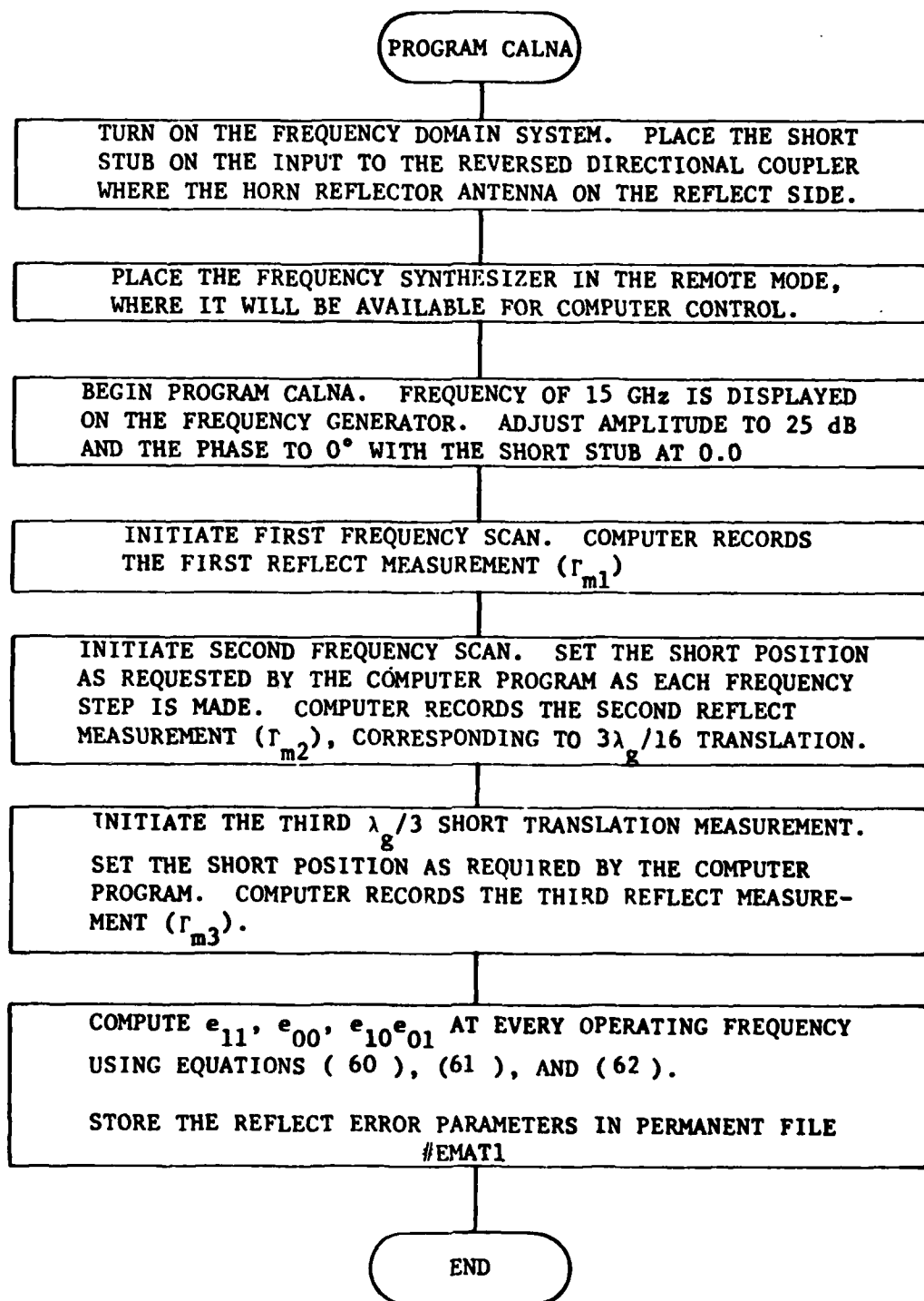


Figure 17. Flowchart of Program CALNA

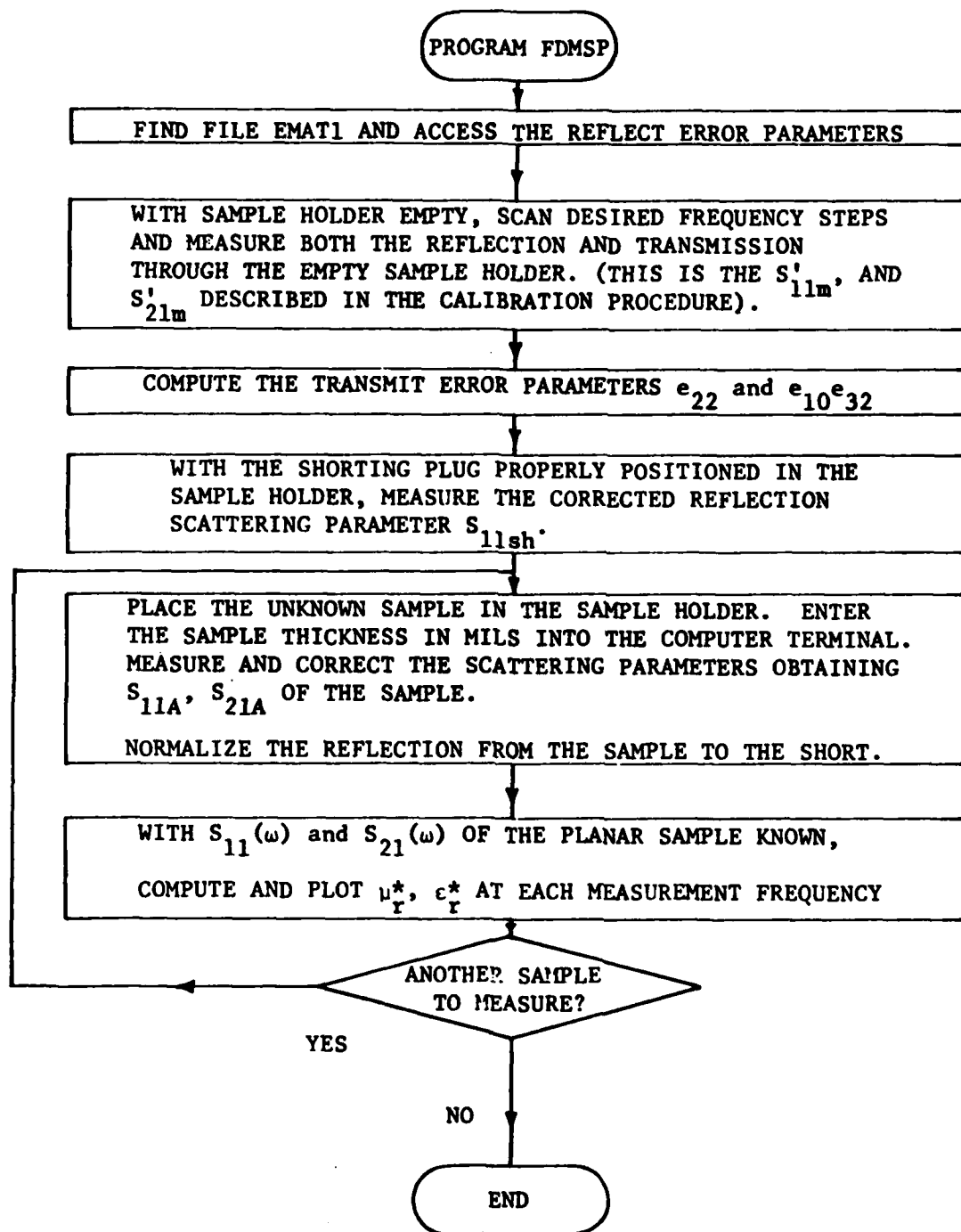


Figure 18. Flowchart of Program FDMSP

The design and procedural discussion of the automated Frequency Domain measurement system is now complete. Note that the only perceptible difference between single and stepped frequency measurements is the actual implementation of the reflect error parameter measurements. The separate calibration program used in the stepped measurement system allows the actual material measurement program to be run quickly in a completely automated fashion.

At this point, the time has come to discuss the actual assembly and evaluation of the Frequency Domain Dual Horn-Reflector Measurement System shown in Figure 15. To begin with, one may notice that the majority of the components shown in Figure 15 are standard Ku-band waveguide components; hence the initial tests were direct towards the dual horn-reflector/sample holder assembly itself. The most fundamental test involved measuring the VSWR of the empty horn-reflector/sample holder across the Ku operating frequency band.

In Section II, it was mentioned that a horn-reflector antenna designed with a small feed flare angle should have a fairly low VSWR. One of the first actual measurements performed on the antenna/sample holder include taking VSWR readings from 12.4 - 18.0 GHz at 50 MHz increments using the test set-up shown in Figure 19. The experimental data is shown in Figure 20. Although many frequencies had a VSWR below 1.10 : 1.0, several frequencies had a VSWR exceeding 3.0 : 1.0. Some of the possible causes of this high VSWR might include: (1) the parabola of the individual horns were designed or constructed incorrectly; (2) physical discontinuities exist between the mounts of the horn-reflector antennas and the sample holder base; or (3) the sample holder supports resonant cavity modes.

First of all, to determine if the high VSWR due to the individual horn-reflector antennas themselves, the sample holder was filled with Ecosorb LS-40 absorber to prevent reflections and transmissions through the sample holder. This experimental set-up is shown in Figure 19. Once again, the VSWR was measured at several frequencies, all of which were below 1.10 : 1.0. The two horn-reflector antennas were then

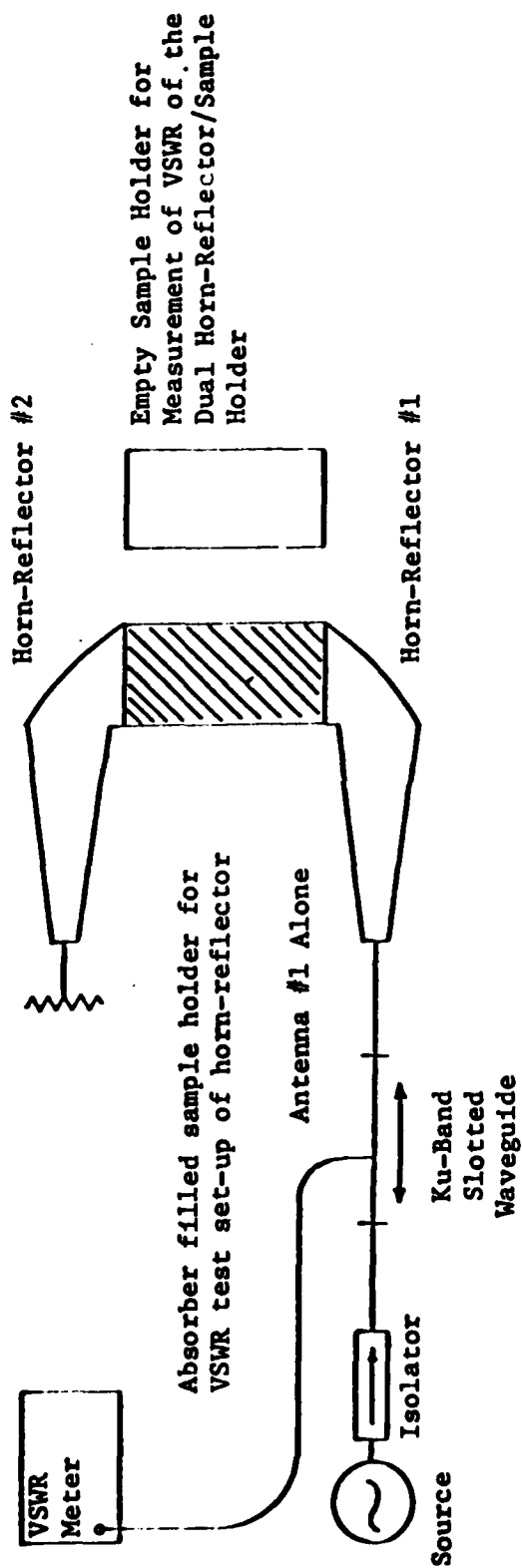


Figure 19. VSWR Test Set-Up

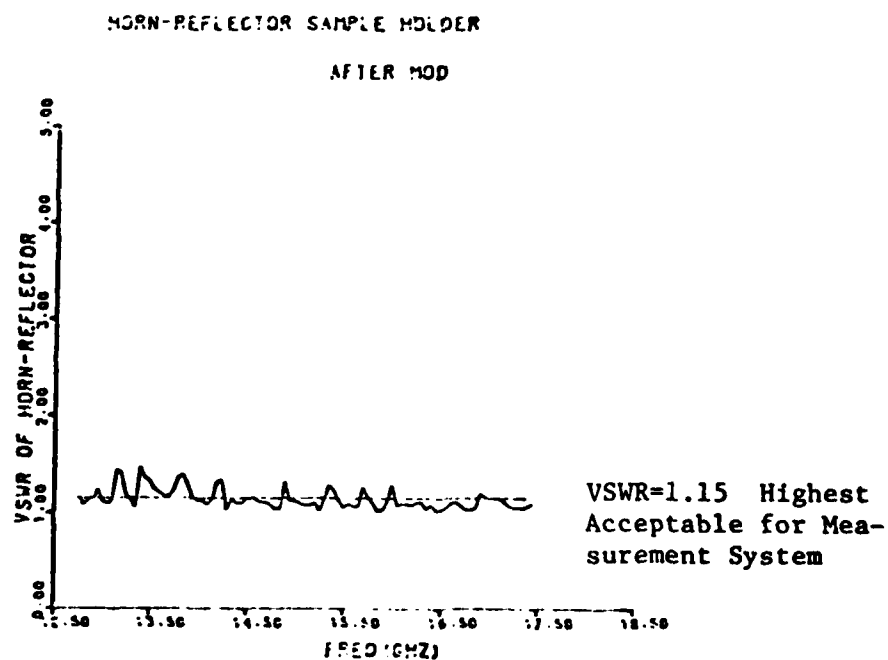
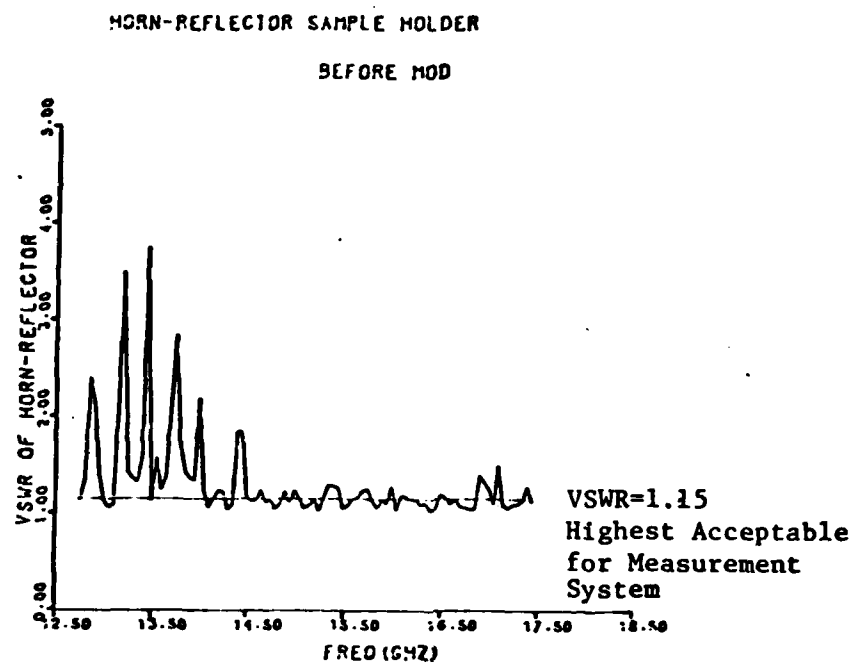


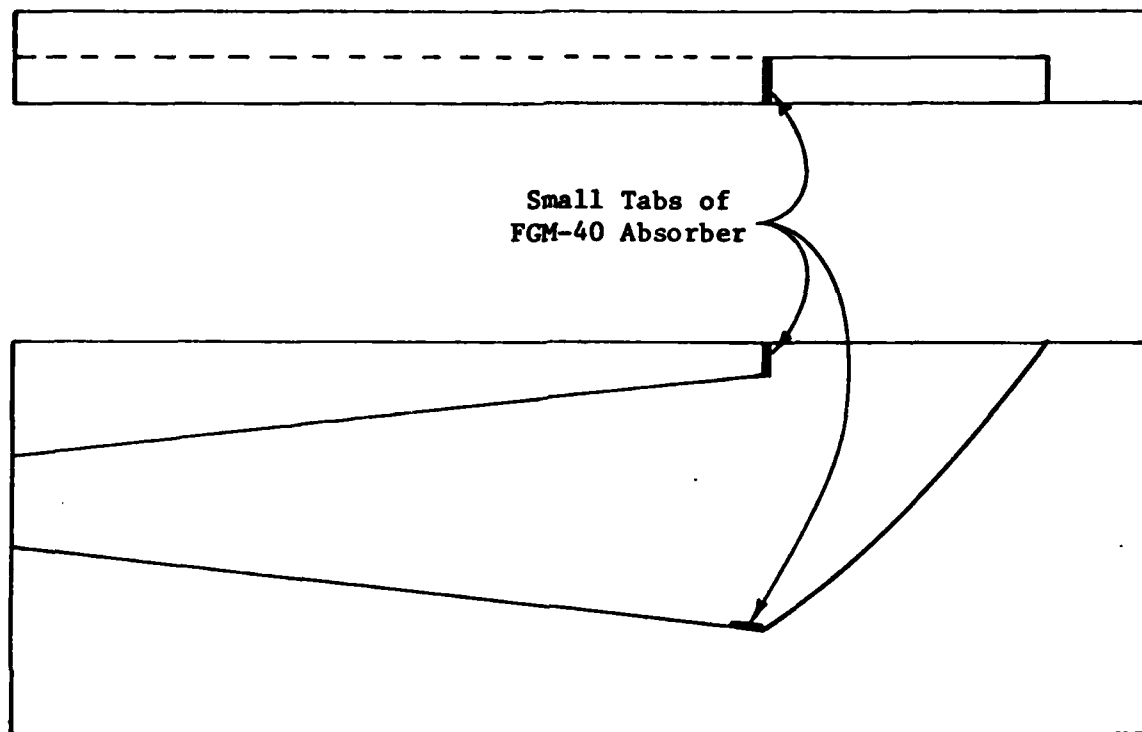
Figure 20. VSWR of Dual Horn-Reflector Before and After the Insertion of FGM-40 Tabs

interchanged, and the measurement repeated with precisely the same results. If the horn-reflector antennas were responsible for the high VSWR, the VSWR would not have changed much when the Ecosorb material was placed in the sample holder, hence the first possibility mentioned in the last paragraph was ruled out.

The second possibility of a poor physical mismatch between the horn-reflector antennas and the sample holder could be checked if the entire assembly is physically inspected with a bright flashlight and an inspection mirror. If any significant physical discontinuity were present, it should have been easy to see with the inspection mirror. Since no such discontinuity was found, the second explanation was ruled out.

The third possible source of a high VSWR may be due to resonant cavity modes which exist in the sample holder itself. It was discovered that the VSWR could be reduced somewhat if a small piece of absorber were placed almost anywhere in the sample holder. Apparently, the absorber perturbed the cavity mode enough so that it disappeared. After some trial and error, it was determined that the resonances were primarily due to the corners where the horn-reflector parabola met the horn sidewalls. To eliminate these resonant modes, small FGM-40 absorber tabs were permanently placed on the suspected corners as shown in Figure 21. After placing the absorber material in the horns, the entire VSWR set-up was reassembled, and the VSWR measurements repeated. The results as shown by the bottom graph of Figure 20 demonstrated that the VSWR was in general significantly reduced across the Ku frequency band. Although at some frequencies the VSWR is still greater than 1.4 : 1.0, there are a sufficient number of frequencies where the VSWR is below 1.15 : 1.0, which is low enough for the purpose of making material measurements. Since it is the intention of this system to make stepped frequency measurements, it is a simple matter to step around those frequencies at which the VSWR is still unacceptable. Over forty frequencies have acceptable VSWR for material measurements, thus this method of reducing the horn-reflector VSWR was acceptable for the time being.





**\*Note: Absorber tabs were place inside both horn reflector antennas**

**Figure 21. Location of Absorber Tabs Used to Reduce VSWR**

Upon completion of the VSWR test, the frequency domain measurement system of Figure 16 was assembled. The next test involved the evaluation of the three-port error correction software described in detail in Section III. In order to check the error correction of the reflect error parameters alone ( $e_{11}$ ,  $e_{00}$ ,  $e_{10}e_{01}$ ), the error parameters were first determined using the calibration procedure described in Section III. Next, an "unknown" device under test was constructed from a Ku waveguide flap attenuator, phase shifter, and short as shown in Figure 22. After measuring the reflection coefficient with no attenuation and phase shift, the technician dialed in an unknown attenuation or phase shift. After reading and computing the corrected reflection coefficient, the enhancement software was able to precisely predict what phase shift or attenuation had been dialed in. Hence, we were satisfied that the reflect error correction software was working as expected.

The checkout of the transmission error parameters proceeded in a similar manner. Using the reflect error parameters found above, the transmit error parameters ( $e_{22}$ ,  $e_{10}e_{32}$ ) were found using the calibration scheme outlined in Section III. With the empty sample holder in place, a second measurement was made of both the reflection and the transmission through the empty sample holder. After correction, the transmission coefficient was unity at an angle of zero degrees, precisely as expected. Next, the shorting block was placed in the sample holder, and the reflection coefficient measured and corrected. Once again, as expected, the amplitude of the reflection coefficient from the shorting plug was .88 or greater at every frequency tested. Hence, we concluded that the total three-port error model was working in a satisfactory manner.

The final test before attempting to use the fully automated measurement system was a check-out of the material measurement ( $\mu, \epsilon$ ) calculation software. In order to check this section out, material measurements had to be attempted at a few spot frequencies. For this test, frequencies of 12.8, 13., 14.8, 16.4, and 17.0 GHz were selected. Teflon was used as the "unknown" sample, since this substance has been measured many times before by the Avionics Laboratory, and its material

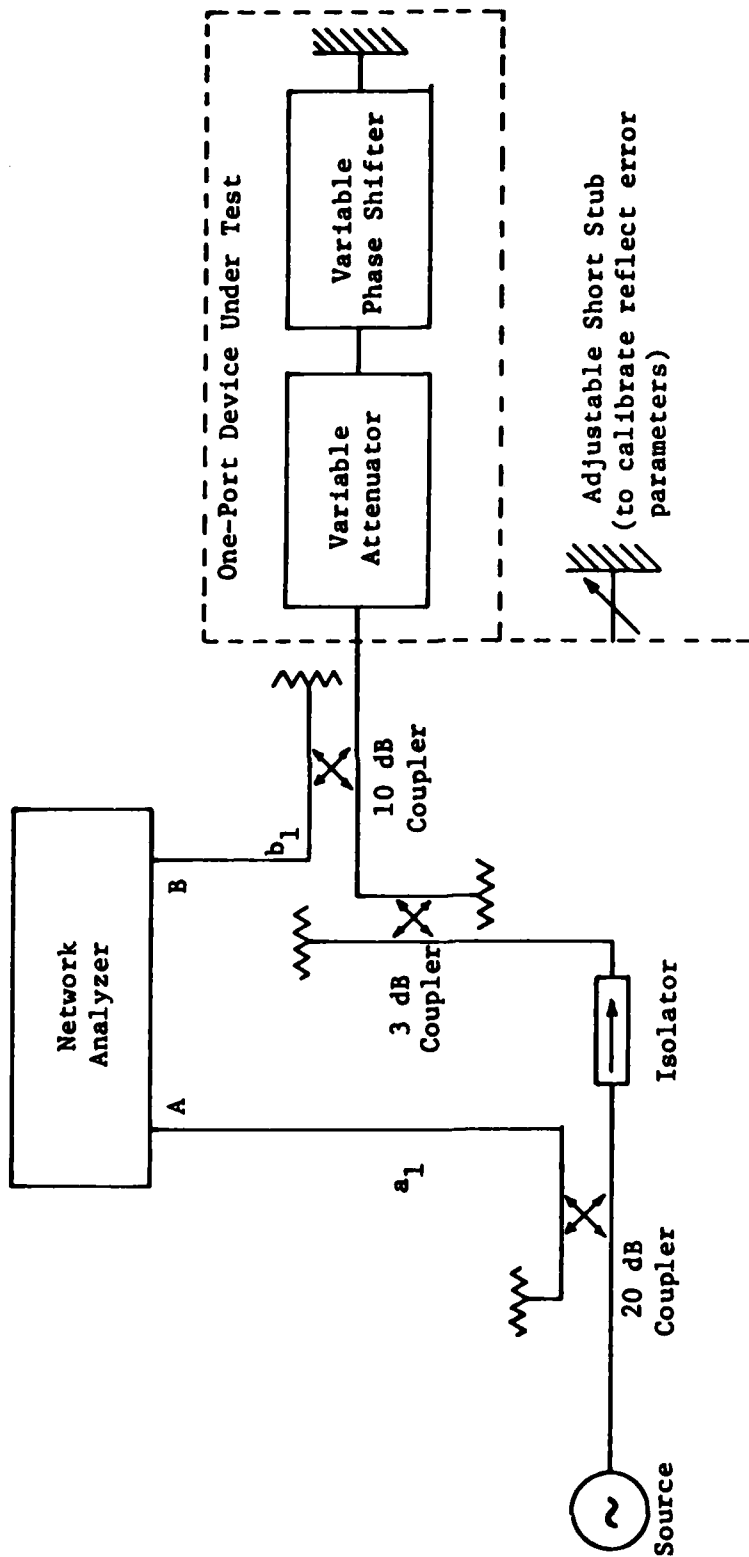


Figure 22. Test and Evaluation Set-Up for Reflect Error Parameter Model

constants of ( $\mu$ ) and ( $\epsilon$ ) are well known. The results of these tests are shown in Table 1. Although a great deal of accuracy was not carried through in these material calculations (some steps were performed on a hand calculator using only three significant figures) this data at least demonstrates that the single frequency material measurement system is working as anticipated. It should be a small matter to get the automated stepped frequency measurement operating, based upon these results. Since single frequency measurements are extremely time consuming, the next subsection shall proceed with the evaluation of the automated measurement system.

Before results are presented of the ( $\mu^*, \epsilon^*$ ) measurement system, some comments must be made about the measurement condition under which the data was assembled. At the time this data was taken, the Watkins-Johnson 1204-1 Frequency Synthesizer was not functioning in the frequency range of 10.0 - 13.0 GHz, hence material measurements were not performed at these frequencies despite the fact that the antenna/sample holder is perfectly capable of measurements at frequencies between 12.6 - 13.0 GHz. From 13.05 - 17.85 GHz, 47 frequencies have been selected for use in the following material measurements. Hence, the five graphs of Frequency Domain data to be compared to Time Domain data represent over 230 single frequency material measurements.

The first measurement performed on the Frequency Domain system is that of air, as shown in Figure 23. As expected the real parts of  $\mu$  and  $\epsilon$  are almost exactly one, with nearly zero imaginary components.

The next sample measured in the frequency domain is the dielectric Teflon, shown in Figure 24. Teflon has an  $\epsilon'$  of approximately 2.05 and an  $\epsilon''$  of about 0. - .100. It is magnetically lossless, hence  $\mu'$  is about 1.0 and  $\mu''$  is 0. Teflon has also been measured numerous times on the Sperry Time Domain Measurement System owned by the Avionics Laboratory. An example of Time Domain data for Teflon is shown in Figure 25. Notice that although the Time Domain data is significantly smoother, it essentially yields the same result. One may note that the Time Domain

TABLE 1  
SINGLE FREQUENCY COMPARISONS OF TEFLON DATA FROM  
TIME DOMAIN MEASUREMENTS AND FREQUENCY DOMAIN MEASUREMENTS

Freq.	Frequency Domain		Time Domain	
	( $\epsilon$ )	( $\mu$ )	( $\epsilon$ )	( $\mu$ )
14.8	2.08 +j .009	1.01 +j .009	1.99 +j .006	1.02 +j 0.00
12.8	2.07 +j .001	.938 +j .009	1.99 +j .012	1.02 +j 0.00
13.00	2.09 +j .060	1.09 +j .050	----	----
16.4	2.08 +j .160	.975 +j .062	2.15 +j .11	.94 +j .003
17.0	2.03 +j .209	.983 +j .089	----	----
17.2	----	----	2.09 +j .20	.960 +j .006

Note: " " Indicates no direct comparison data is available. The average value for the ( $\epsilon, \mu$ ) of Teflon is roughly (2.02 +j 0.05, 1.00 +j 0.0)

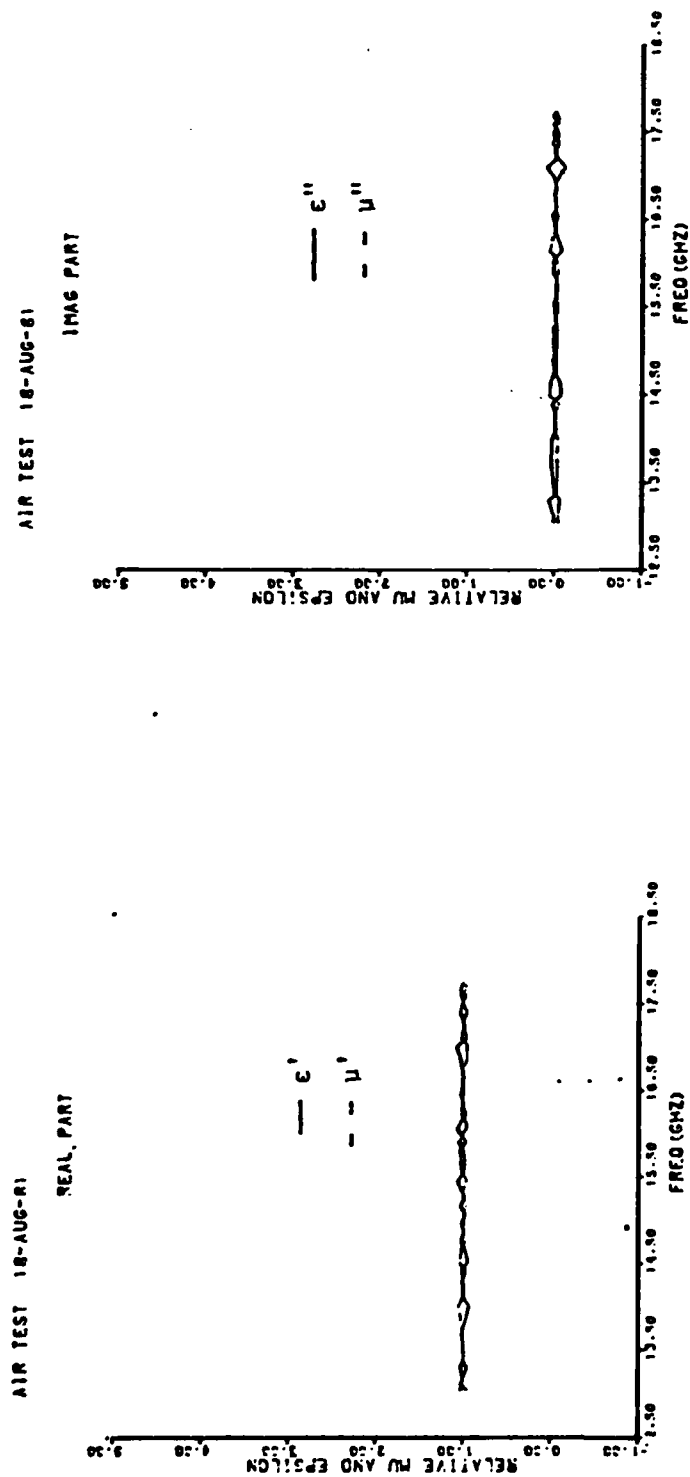


Figure 23. Mu-Epsilon of Air (Frequency Domain)

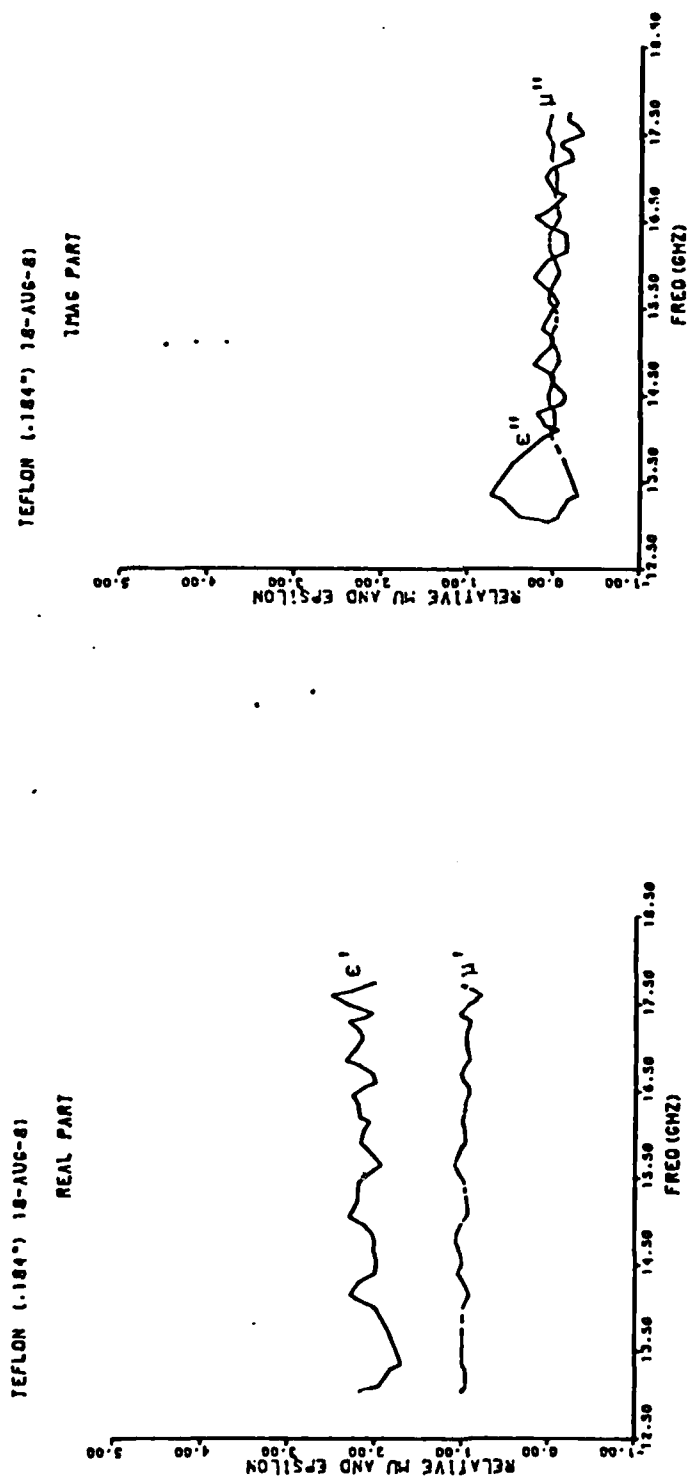


Figure 24. Mu-Epsilon of Teflon (Frequency Domain)

SAMPLE: TEFLON( 202°) 8-18-81 TIME DOMAIN

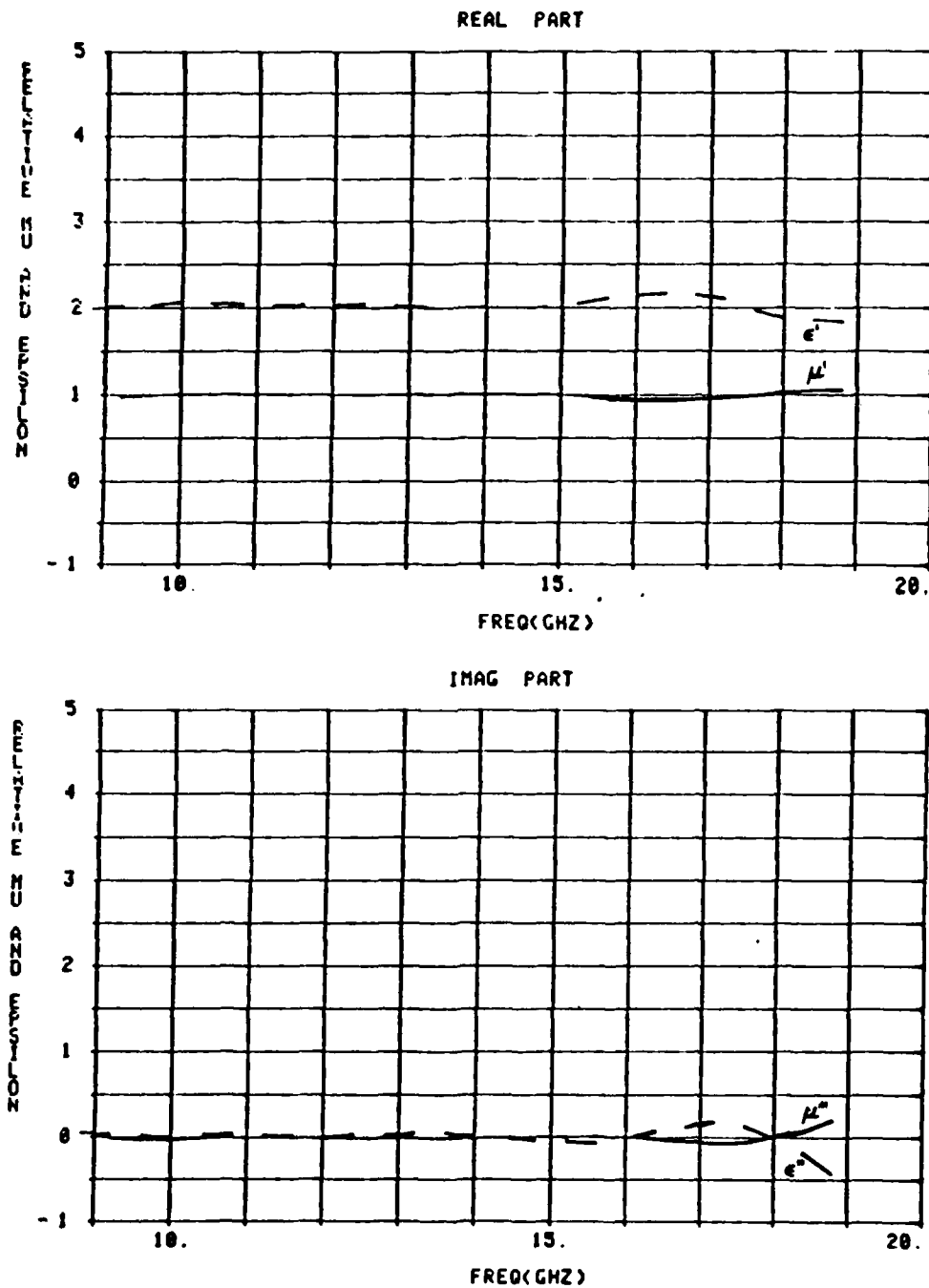


Figure 25. Mu-Epsilon of Teflon (Time Domain)



data presented has only 24 data points from 9.0 - 18.5 GHz, while the Frequency Domain data has 47 data points from 13.05 - 17.75 GHz.

The next sample to be compared is a thin sample of plexiglas. The permittivity and permeability as measured by the Frequency Domain system is shown in Figure 26. Notice that besides a large irregularity in the data about 13.3 GHz, the  $\epsilon'$  is about 2.65 and the  $\mu'$  is about 1.0. The imaginary component, though a little noisy, is still about 0.0 - 0.2 at most frequencies. The Sperry Time Domain data for plexiglas is shown in Figure 27. Note that  $\epsilon'$  is about 2.6 and  $\mu'$  is about 1.0. Their respective imaginary components  $\epsilon''$  and  $\mu''$  are roughly .1 and 0., respectively. Thus, there is a good comparison between the time and frequency domain data for this particular sample.

Fiberglass constituted the fourth sample to be measured and compared by the time and frequency domain system. Figure 28 is a plot of  $\mu$  and  $\epsilon$  from a sample of fiberglass. Unlike the previous sample, this particular material had data which varied considerably in  $\epsilon'$  and  $\epsilon''$ , but varied little in  $\mu'$  and  $\mu''$ . Since the fiberglass sample used in the frequency domain system is not a completely homogeneous substance, these variations may be partly due to the surface roughness of the sample. (Note - the time domain uses 14 mm coaxial samples and the frequency domain uses rectangular samples.) If a few of the large peaks in the data we ignored in  $\epsilon'$ , most of the values lie close to 4.2 in magnitude. The permeability, however, is still almost 1. Compare these measurements to the Time Domain data for Fiberglass presented in Figure 29. Although the real part of  $\epsilon'$  is much smoother in the time domain, its average value is still about 4.2. Looking at the  $\epsilon''$  data, it also varies somewhat, but not quite as much as the frequency domain data. Despite this variation, the  $\mu'$  and  $\mu''$  of both the time and frequency do compare quite well for this material.

At this point, one may wonder why in general frequency domain data tends to be noisier than the time domain data. One major contributing cause may be the phase/amplitude display plug-in for the HP 8410B Network Analyzer. When a phase angle approaches plus or minus 180°, the

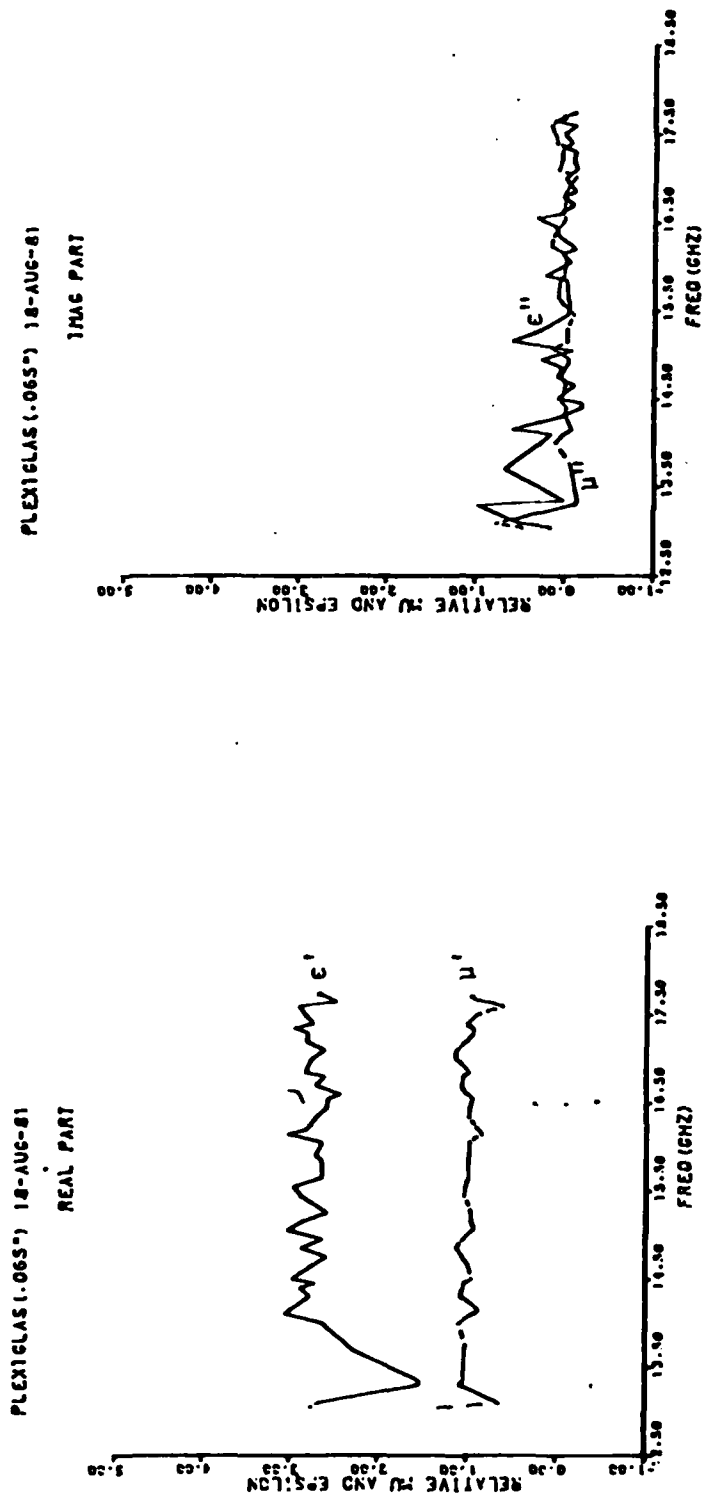


Figure 26. Mu-Epsilon of Plexiglas (Frequency Domain)

SAMPLE: PLEXIGLAS(.0645") 8-18-81 TIME DOMAIN

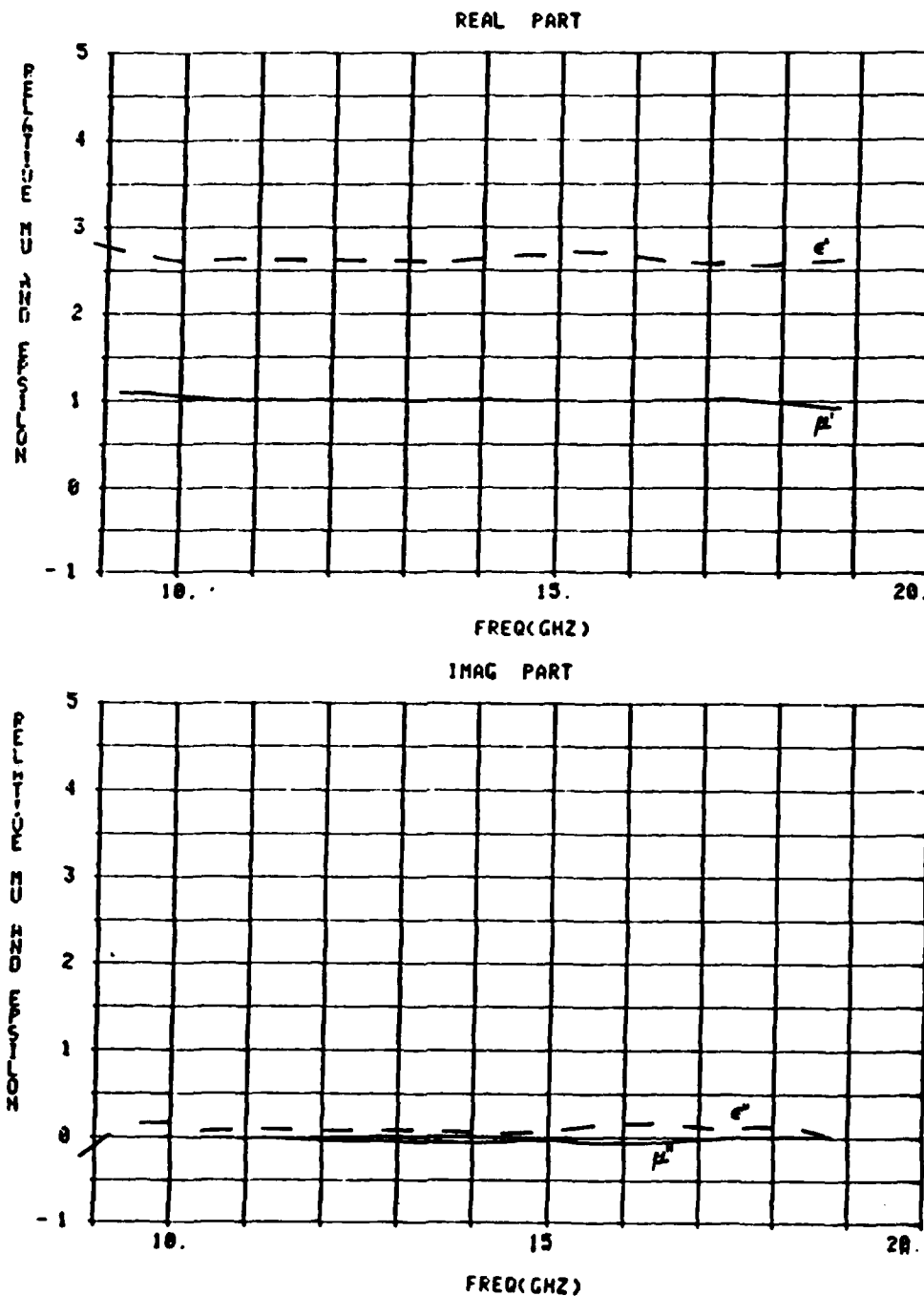


Figure 27. Mu-Epsilon of Plexiglas (Time Domain)

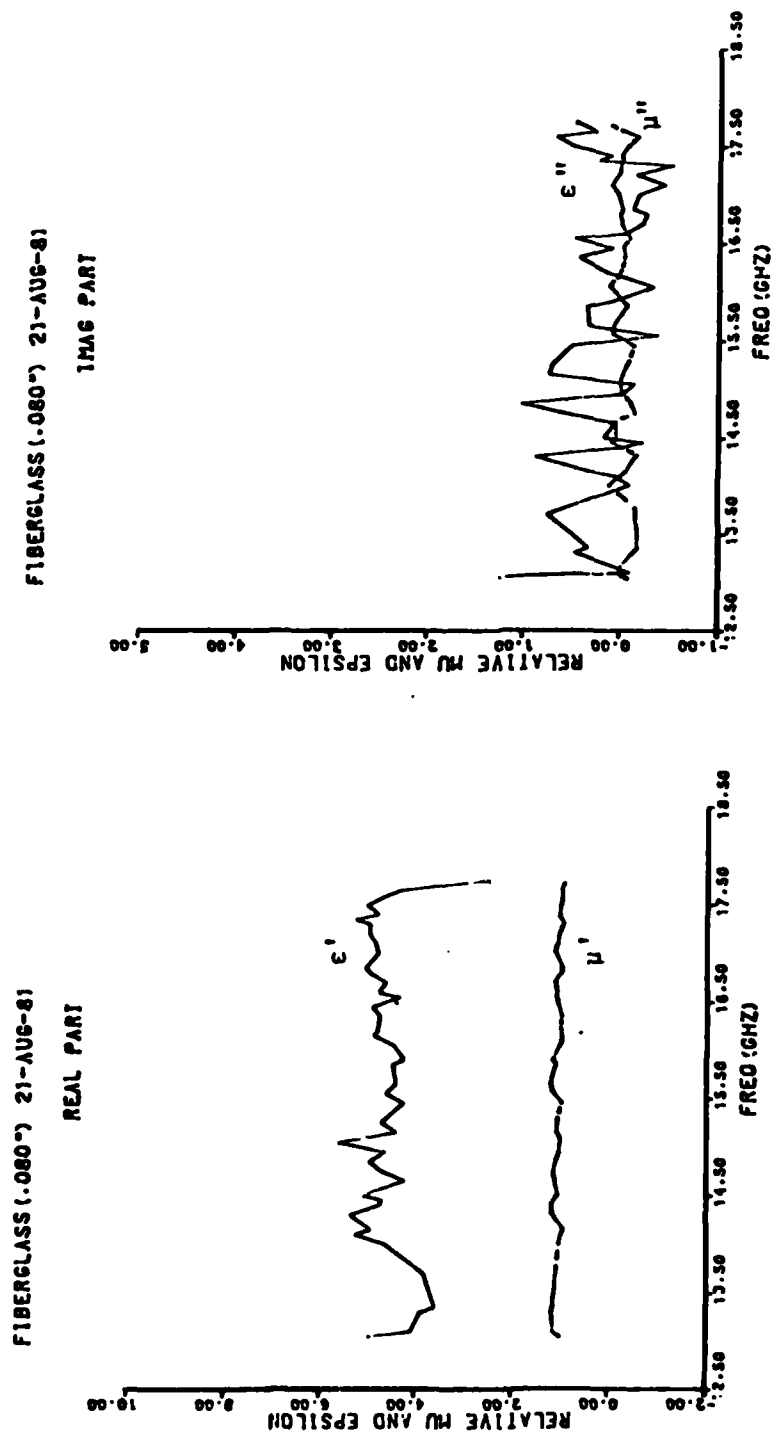


Figure 28. Mu-Epsilon of Fiberglass (Frequency Domain)

SAMPLE: FIBERGLASS(.1345") 8-18-81 TIME DOMAIN

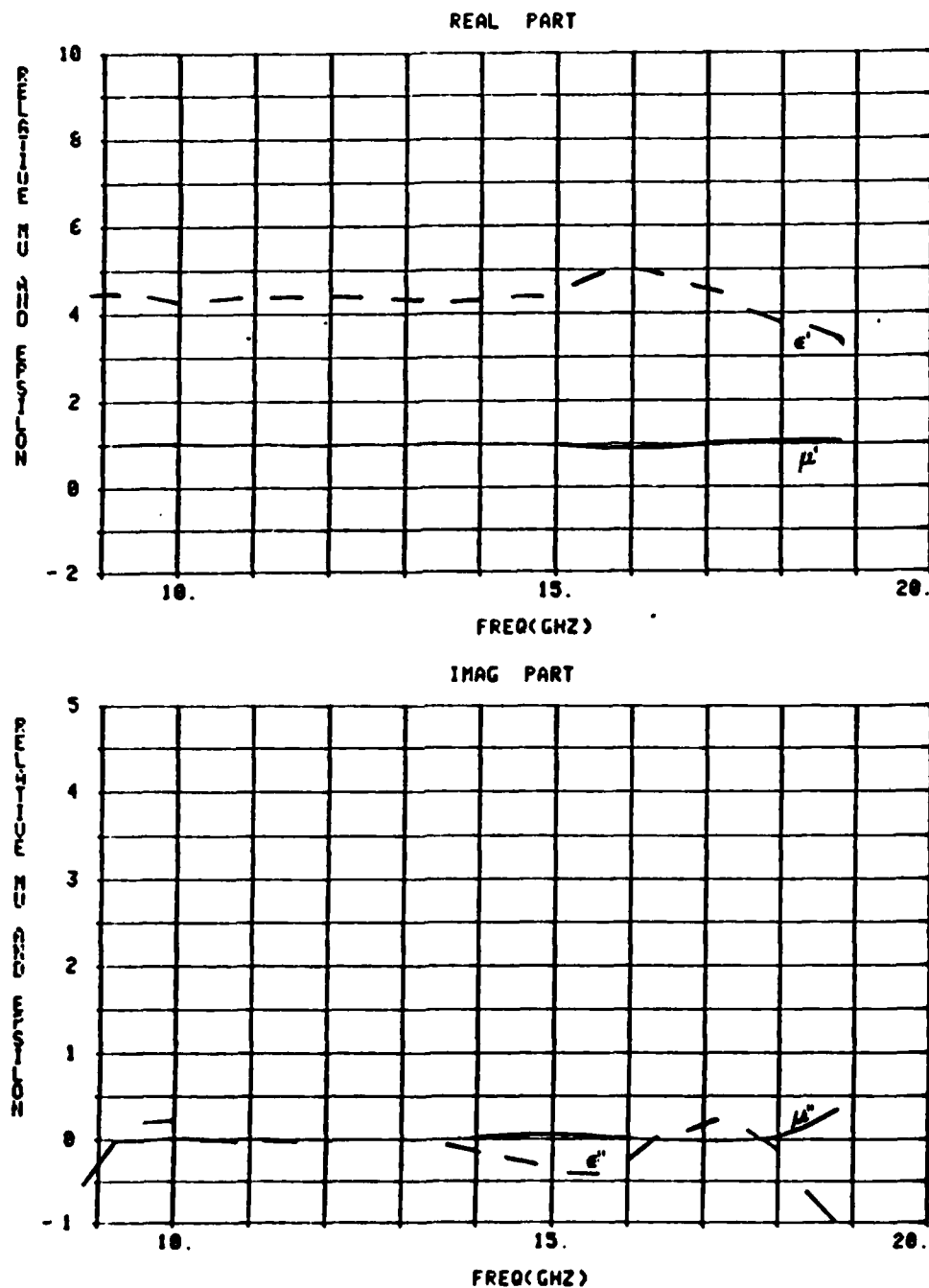


Figure 29. Mu-Epsilon of Fiberglass (Time Domain)

display needle for the phase becomes very unsteady as the angle switches the entire range from minus to plus 180°. Thus, a phase angle measurement of 179.6° might be actually read by the computer as almost any angle between plus and minus 180°. Suppose the computer took for a phase measurement 81° instead of 179.6°. Due to the complex interrelation between  $(\mu^*, \epsilon^*)$  and  $S_{11}, S_{21}$ , this induces a big error in the  $(\mu^*, \epsilon^*)$  calculation. On the graph of mu and epsilon versus frequency, this shows up as a big spike in the data. The solution to this problem would be to obtain a polar display plug-in for the Network Analyzer, which puts out the phase angle continuously from 0 - 360°, instead of minus 180° to plus 180°.

Before closing this section, a few general comments will be added about the measurement of lossy absorbing materials. It is well known that absorber materials are difficult to precisely manufacture in large quantities with consistent quality control. Two samples taken from the same sheet of absorber may have a 20 - 50 percent variance in absorber properties. If an absorber is heated or compressed, its material properties may also change drastically. With this in mind, let us investigate the  $(\mu, \epsilon)$  of two samples of a typical production absorber, Ecosorb LS-40. From Figure 30, this sample has an  $\epsilon'$  of about 1.6 and a  $\mu'$  of about 1, as measured in the frequency domain. On the imaginary side,  $\epsilon''$  is about 1.1 - 1.3 with a  $\mu''$  of about 0.0. Compare this sample of LS-24 with that of a coaxial sample measured on the Sperry Time Domain System, as shown in Figure 31. The time domain  $\epsilon'$  and  $\mu'$  is roughly 2. and 1., respectively, while the  $\epsilon''$  varies from 2.0 to 1.0. The imaginary permeability is about 0.0, which is expected for this non-magnetic absorber. These two samples came from the same sheet, yet the real and imaginary portion of  $\epsilon^*$  are slightly different.

Once final note must be made at this point. The mu-epsilon calculation routine cannot handle samples which are electrically thicker than one quarter wavelength. To get an idea of how thick the sample should be, take the free space wavelength and divide by the square root of the estimated real part of epsilon. The sample thickness should not be more than one quarter of this number.

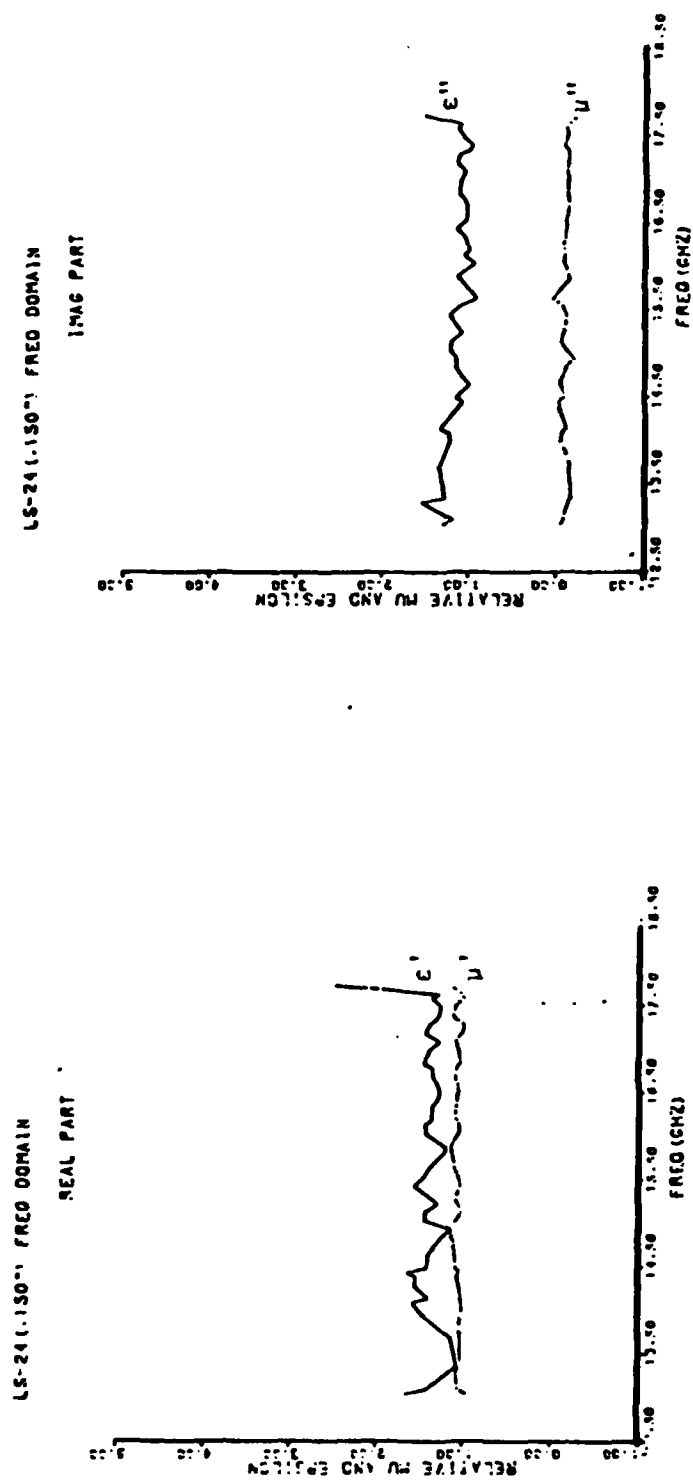


Figure 30. Mu-Epsilon of LS-40 Absorber (Frequency Domain)

SAMPLE: LS-24 150 MILS TIME DOMAIN 8-18-81

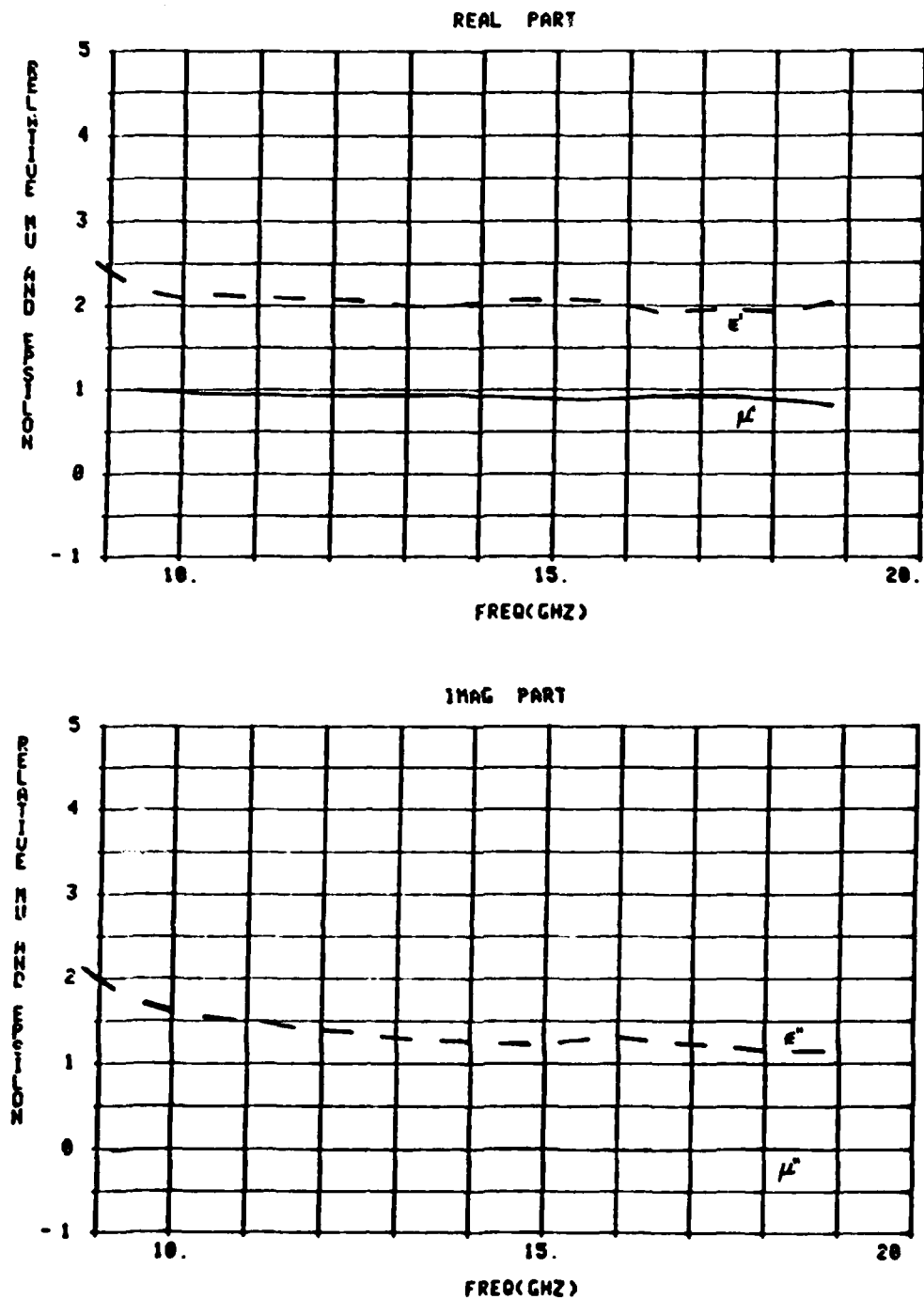


Figure 31. Mu-Epsilon of LS-40 Absorber (Time Domain)



## SECTION V

### SUMMARY AND CONCLUSIONS

The overall results of this thesis investigation may be summarized as follows. A practical wideband permittivity and permeability automated measurement system can be constructed in the Ku (12.4 - 18.0 Gigahertz) frequency band. Such a system consists of a three-port reflectometer, network analyzer, frequency synthesizer, and a dual horn-reflector/sample holder. To correct for non-ideal waveguide components and directional couplers, a three-port "error adaptor" is included in the mathematic model of the microwave circuit. A calibration procedure is included to calibrate both the error adaptor and the entire Frequency Domain Measurement System. Finally, a comparison between  $(\mu, \epsilon)$  data obtained in this Frequency Domain system and the Sperry Time Domain system demonstrated that the two measurement systems produced results which were within ten percent of each other, thus verifying the correct operation of the Frequency Domain system.

At the present, the Avionics Laboratory has the capacity of measuring  $(\mu, \epsilon)$  by the two completely different methods from 12.4 - 18.0 Gigahertz. In the future the Avionics Laboratory intends to purchase the required up and down frequency converters to extend the Frequency Domain System above 18.0 Gigahertz, a frequency range which cannot be covered by the current Time Domain System. Hence by demonstrating the ability to make Frequency Domain  $(\mu, \epsilon)$  measurements in the Ku band, this investigation has laid the groundwork for possible automated frequency Domain measurements above 18.0 Gigahertz.

In conclusion, this section has discussed how to assemble a practical scattering parameter measurement set-up. It also discussed some of the initial problems that were encountered when the system was first installed. Finally, the section ended by comparing measured ( $\mu^*$ ,  $\epsilon^*$ ) data between the Time Domain Measurement System and the Dual Horn-Reflector Measurement System developed in this thesis. The average system accuracy is above ninety percent at most of the operating frequencies, based upon the data comparisons between the time and frequency domain measurement systems.

## APPENDIX A

### ENGINEERING DRAWINGS OF DUAL HORN-REFLECTOR/SAMPLE HOLDER

This appendix contains all of the final engineering drawings of the Horn-Reflector/Sample Holder arrangement. Included in the following figures are the reflector antenna base, the reflector antenna cover, the sample holder base and cover, the shorting plug and stub, and the gage positioning block.

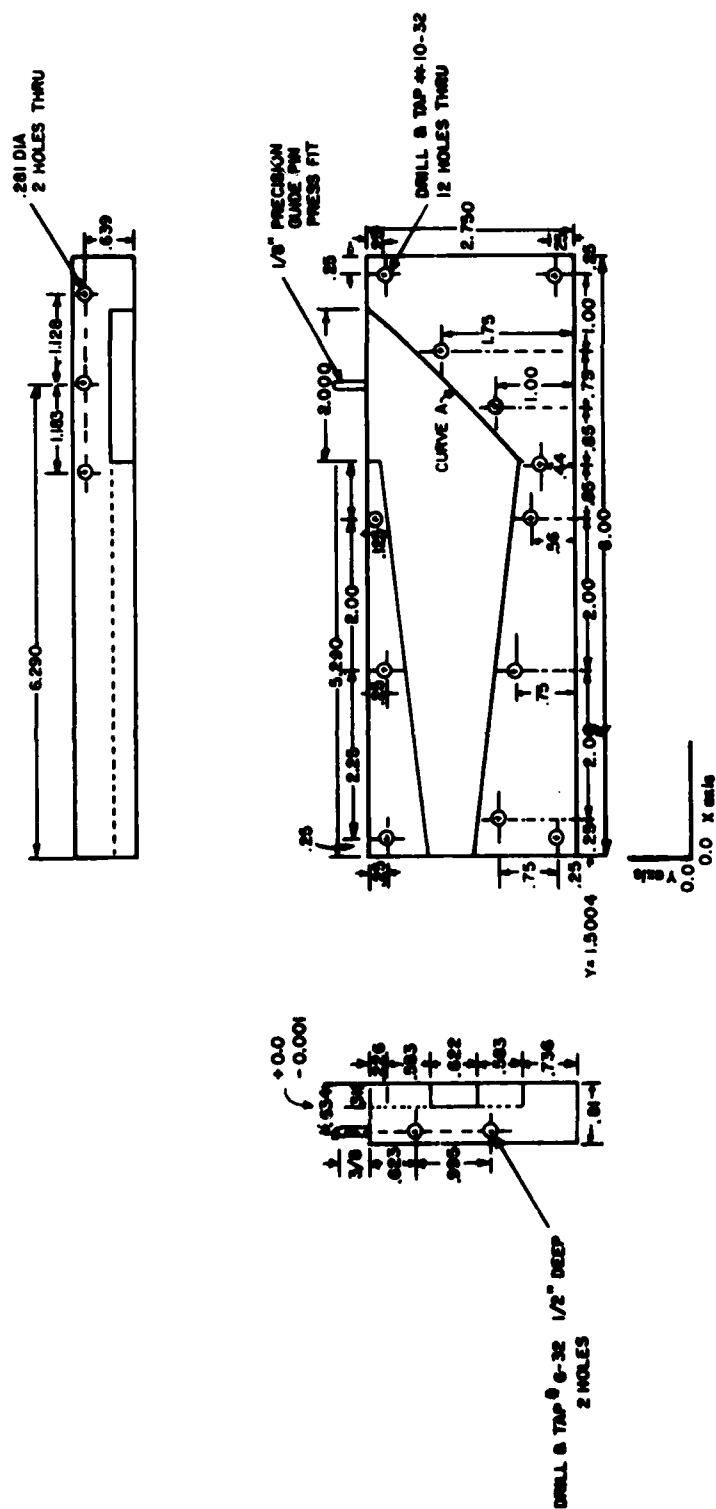


**Figure 32. Horn-Reflector Antenna Center Piece**

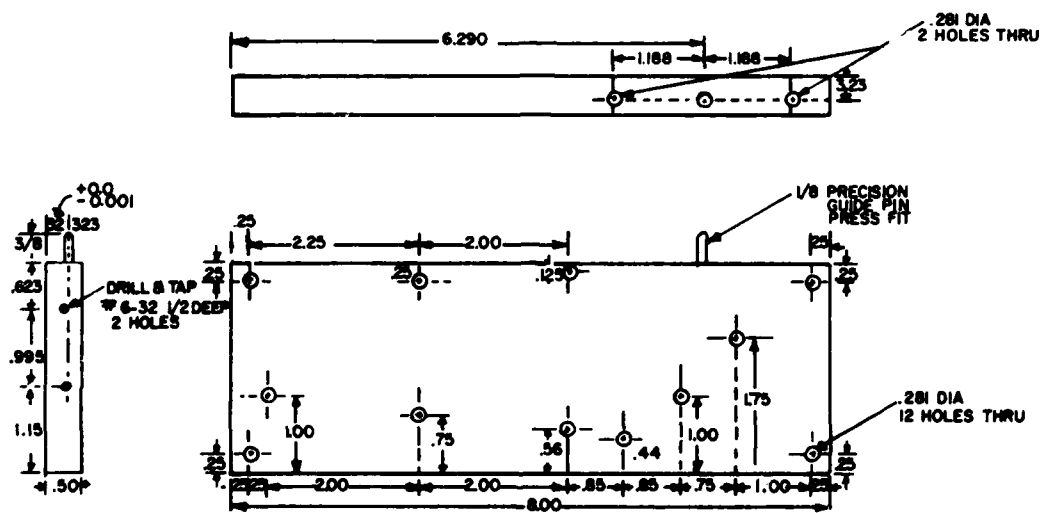


Figure 33. Horn-Reflector Antenna Cover

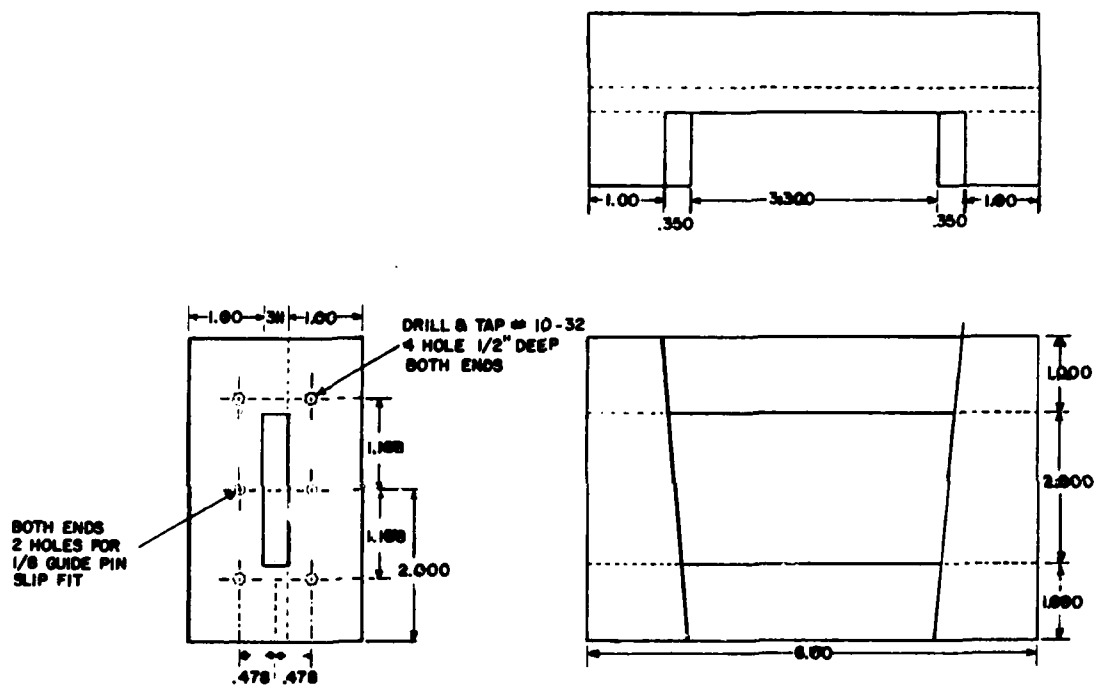


Figure 34. Sample Holder Base Without Cover

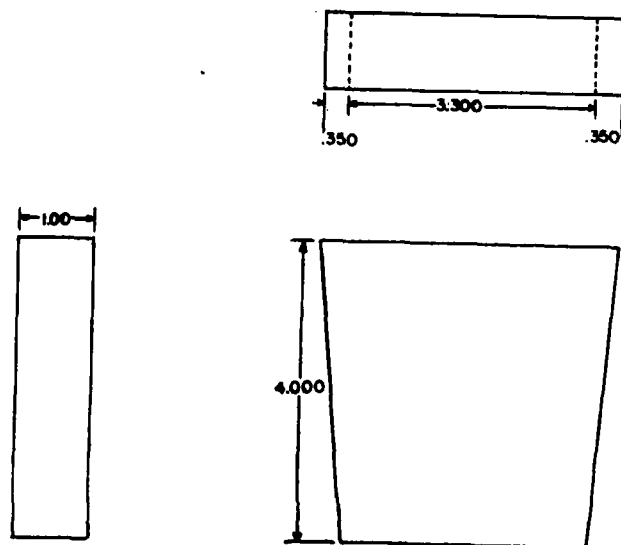


Figure 35. Sample Holder Cover

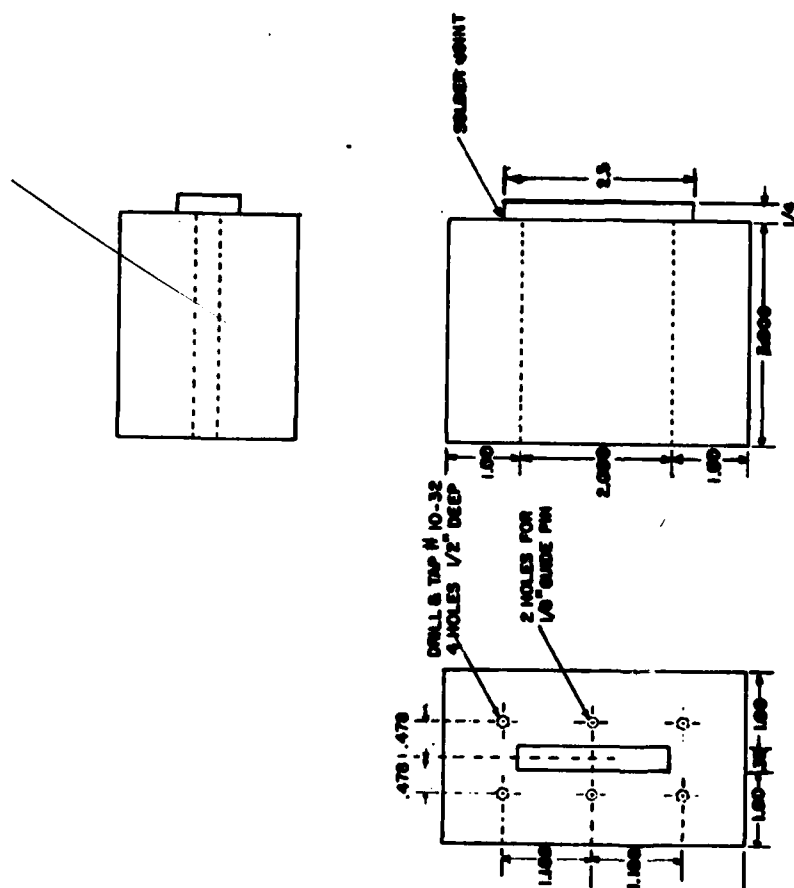
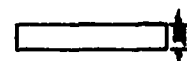
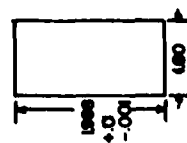
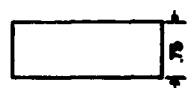
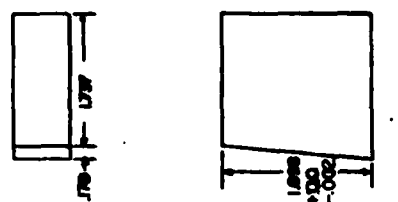


Figure 36. Shorting Stub





A B

Figure 37. Shorting Plug (A-Side) and Gage Block (B-Side)

REFERENCES

1. Nicolson, A., Time Domain Measurements of Microwave Absorbers, Sperry Rand Research Center, Sudbury, Massachusetts, Avionics Laboratory Contractor Report AFAL-TR-71-33, February 1971.
2. Nicolson, A., Mitchell, R., Aukenthaler, A., Time Domain Measurements of Microwave Absorbers, Sperry Rand Research Center, Sudbury, Massachusetts, Avionics Laboratory Contractor Report AFAL-TR-71-353, November 1971.
3. Kent, B., Time Domain Measurements of Microwave Absorbers With Real Time Processing, Avionics Laboratory, W-PAFB, Ohio, AFAL Tech Memo AFAL-TM-79-3, March 1979.
4. Collin, R. E., Field Theory of Guided Waves, McGraw Hill Book Company, New York, 1960, pg 76-91.
5. Nyquist, D. P., EE-836 Class Notes on Electromagnetic Waves, Michigan State University Engineering Press, East Lansing, Michigan, Chapter 3, pg 29-33.
6. Aguirre, D. G., Captain, USAF, Frequency Domain Measurements of Microwave Absorber Design Materials, A thesis prepared for the Air Force Institute of Technology, AFIT/GE/EE/80D-8, December 1980.
7. Crawford, A., Hogg, D., Hunt, L., "A Horn Reflector Antenna for Space Communications," The Bell System Technical Journal, July 1961, pg 1095-1116.
8. Mentzer, C. A., Analysis and Design of High Beam Efficiency Aperture Antennas, A Dissertation prepared for the Ohio State University Department of Electrical Engineering, Columbus, Ohio, 1974. Work supported by the National Science Foundation, under grant GK-33974.
9. Kraus, J., and Carver, K., Electromagnetics, McGraw Hill Book Company, New York, Second Edition, 1973, pg 528-529.
10. Nicolson, A. op. cit.
11. "Vector Measurements of High Frequency Networks," Hewlett-Packard Technical Seminar, H-P Part Number 5952-9270, May 1978.
12. Anderson, R., "S-Parameter Technique for Faster More Accurate Network Design," Hewlett-Packard Technical Journal, February 1967. Also published as HP Applications Note 95-1.
13. "Semi-Automated Measurements Using the 8410B Microwave Network Analyzer, and the 9825A Desk Top Computer," Hewlett-Packard Application Note 221, October 1977.

REFERENCES (Concluded)

14. Rytting, D., "Analysis of Vector Measurement Accuracy Enhancement Techniques," Hewlett-Packard Technical Seminar, Transcript available through the author at Hewlett-Packard, 1400 Fountain Grove Parkway, Santa Rosa, California.